Andreas Theiler, BSc

# Localisation of Majorana fermions in ferromagnetic impurity chains on spin-orbit coupled superconductors

**MASTER'S THESIS**

to achieve the university degree of

Diplom-Ingenieur

Master's degree programme: Technical Physics

submitted to

**Graz University of Technology**

Supervisor

Univ.-Prof. Dipl.-Phys. Dr.rer.nat., Wolfgang von der Linden

Institut für Theoretische Physik - Computational Physics

Annica Black-Schaffer
Department of Physics and Astronomy - Uppsala University

Graz, June 2018

## AFFIDAVIT

I declare that I have authored this thesis independently, that I have not used other than the declared sources/resources, and that I have explicitly indicated all material which has been quoted either literally or by content from the sources used. The text document uploaded to TUGRAZonline is identical to the present master's thesis.

_____       _____

          Date                                            Signature

# Abstract

We are considering a two-dimensional s-wave superconductor with spin-orbit interaction coupled to a ferromagnetic adatomic chain. This particular system is already well-known for hosting Majorana fermion states from theoretical studies as well as experiments. By adjusting the coupling between the ferromagnetic impurities and the host superconductor we tune the system into a topological non-trivial phase, thus introducing zero energy states in the system, which can be identified as Majorana fermions. The system was simulated using the tight binding tool kit, a self-consistent approach to calculate the local variations in the superconducting order parameter and the Chebyshev expansion method for determining the local density of states. We are particularly interested in studying the influence of the self-consistent approach on the simulation results and comparing it to a constant order parameter approximation. Furthermore, we are showing that the localisation of the Majorana fermions can be described using edge states and that Majorana fermion states can hybridise with other states for certain ferromagnetic coupling strengths.

# Kurzfassung

In dieser Arbeit wird ein zweidimensionaler, konventioneller Supraleiter mit Spin-Bahn-Wechselwirkung betrachtet, welcher zusätzlich an eine ferromagnetische Störstellenkette gekoppelt ist. In theoretischen Überlegungen sowie in Experimenten wurde bereits gezeigt, dass in diesem speziellen System Majorana-Fermion-Zustände auftreten. Durch Anpassung der Kopplung zwischen den ferromagnetischen Störungen und dem Substratsupraleiter wird das System in eine topologische, nicht-triviale Phase gebracht. Dadurch werden im System Null-Energie-Zustände eingeführt, welche als Majorana-Fermionen identifiziert werden können. Das Systems wurde mittels des Tight-Binding-Tool-Kits simuliert, wobei ein selbstkonsistenter Ansatz zur Berechnung der lokalen Variationen des Ordnungsparameters sowie die Chebyshev-Expansions-Methode zur Berechnung der lokalen Zustandsdichte verwendet wurden. Besonderes Augenmerk wurde auf den Einfluss des selbstkonsistenten Ansatzes auf die Ergebnisse gelegt, wobei diese mit den Lösungen der konstanten Ordnungsparameter-Näherung verglichen wurden. Weiterhin wird gezeigt, dass die Lokalisierung der Majorana-Fermionen mit Hilfe von Randzuständen beschrieben werden kann und dass Majorana-Fermion-Zustände für bestimmte ferromagnetische Kopplungsstärken mit angeregten Zuständen hybridisieren.

# Contents

Contents

# List of Figures

# 1 Introduction

Majorana fermions were first envisioned by Ettore Majorana in 1937, by solving the Dirac equation using real valued particle fields [1]. These exotic particles have the intriguing property of being their own antiparticle, unlike conventional fermions such as electrons or protons. So far, there have been no indications in high energy experiments that these exotic particles exist in nature. However, Majorana himself [2] and unified field theories [3–5] proposed that the neutrino might be a Majorana fermion and there are further theories predicting the existence of such particles due to supersymmetry [2, 6, 7].

In condensed matter physics, the picture is somewhat different and Majorana fermions can be found in the form of quasiparticles in certain materials [2]. They are of particular interest for quantum computing applications because they are anyons which show a so a called non-Abelian behaviour [8–10]. It has been demonstrated that in theory one can build a quantum computer using such particles [11]. An intriguing property of the Majorana fermions thereby is that they are predicted to be particularly stable in such applications [12].

Edges states, found in topological phases of matter, can provide particle energy spectra analogue to the Dirac spectrum for relativistic particles and are a natural hunting ground for Majorana quasiparticles [13]. Such systems, among others, include topological insulators [14, 15], quantum wires made out of semiconductors [16–18] and ferromagnetic impurity wires doped on superconductors [19–27]. The latter system being in the focus of this work. This system is in particular appealing since it consists of two components, a spin-orbit coupled $s$-wave superconductor and a ferromagnetic adatomic chain, both with experimentally easily accessible properties of common materials. For example, lead can be used as the superconducting host material and iron atoms as the ferromagnetic impurities. Using these two materials, several experiments were conducted and found strong indications that Majorana fermions are present in such

1

a system [28–31].

There are still some open questions when it comes to simulations of this particular system and we will address three of them in this thesis.

First, we will discuss the self-consistent method which is used to simulate the suppression of the superconducting order parameter through the applied magnetic interaction. This method is computationally significantly more expensive than a non-self-consistent approximation, but it is considered to provide a more accurate representation of the spatial order parameter distribution. We will compare both methods in order to see if the additional computing effort for the self-consistent approach is justified.

Previous theories link the localisation of the Majorana fermions to the coherence length of the superconductor [32–34], which predict the opposite trend to our simulations with respect to increasing ferromagnetic coupling strengths. We will show that deriving the localisation from edge states [26, 35, 36] will yield the right tendency.

Lastly, we will explain how Majorana fermions can hybridise with other states, altering their typical characteristic of being a zero energy state.

The remainder if this thesis will be structured as follows: In the theory Chapter 2, the microscopical concepts behind conventional superconducting in its mean field formulation is introduced. We will further provide a definition for Majorana fermions in solid state physics and explain the core concepts of topology in band structures. Eventually, by combining superconductivity with topology, we will analyse why a ferromagnetic wire doped on a spin-orbit coupled superconductor will lead to Majorana states at the ends of the wire.

In the methods Section 3, a real space Hamiltonian describing the system, is introduced. To extract the local density of states, the tight binding tool kit [37] in combination with the Chebyshev expansion method [38, 39] was used. The spatial variations of the superconducting order parameter were simulated, using a self-consistent calculation.

The results Chapter 4 shows the behaviour of the system under the alteration of important parameters and is concerned with answering the beforehand mentioned questions.

Finally, the conclusion 5 will provide a short summary of the thesis.

# 2 Theory

## 2.1 Prerequisites

This chapter aims to give the reader an overview over the core concepts needed to understand the physics behind topological superconductivity and Majorana fermions. We will start out with an introduction to conventional superconductivity, which eventually will introduce so called Bogoliubov quasiparticles, a key ingredient for Majorana fermions in topological superconductors. Having introduced these particular quasiparticles we will define and discuss Majorana fermions in solid state physics. Next, the reader is familiarised with important concepts of topological band structures and, finally, all these concepts are joined in order show how Majorana fermions can be created with the help of a ferromagnetic wire doped on a superconductor.

These physical concepts will be explained in a short and concise manner in this chapter. Therefore, if a deeper understanding of the topic is desired, we would recommend some of the following literature. For a general introduction to many body physics, the books [40–43] are a good starting point. Core concepts of superconductivity are explained well in references [44–46]. The mathematical field of topology is discussed in the books [47, 48] and its application to band structures and, eventually, Majorana fermions can be found in references [10, 26, 35, 36, 49–52]. A popular science paper about Majorana fermions we would like to call attention to is "Majorana returns" by Wilczek [2].

For the best reading experience of this introduction to topological superconductivity and Majorana fermions, the reader should have basic knowledge of the following topics. First of all, our discussions will mainly be focused on band structures, obtained by tight binding models. A good explanation for these solid state physics concepts can be found in the books [53–55]. Furthermore, most concepts will be described using the

language of second quantisation. A good introduction to this topic can be found in many body physics books [40, 42, 43] as well as in introductory books to quantum field theory [56–58].

While the core concepts of topological superconductivity introduced in this chapter are aimed to be understandable with this particular background, some interesting details, usually pointed out in the footnotes, might require a deeper knowledge.

It is also noteworthy that natural units will be used throughout this thesis ($\hbar = 1$ and $c = 1$) and, if not stated otherwise, all calculations are implemented at zero temperature.

## 2.2 Theory of superconductivity

### 2.2.1 Introduction

In a nutshell, superconductivity is a phase that a material can transition into at a certain critical temperature, which in general is within the order of a few Kelvin. Below this critical temperature, the material loses its electrical resistivity completely and resembles a perfect conductor. Another interesting feature of the superconducting phase is that it expels magnetic fields from the bulk of the material, which is known as the Meisner effect and cannot be explained by the loss of electrical resistance alone[1]. Superconductivity was first discovered by Kamerlingh Omnes in 1911 [59] by cooling mercury with liquid helium.

It took 46 years after the discovery of superconductivity to find a microscopic theory which was able to describe this phenomenon sufficiently. In 1957, Bardeen, Cooper and Schrieffer (BCS) published their famous work about a microscopic theory which was able to sufficiently describe superconductivity [60]. The theory is still very successful as it describes a wide range of superconductors, nowadays known as conventional superconductors.

---

[1]The cause of this effect is linked to the spontaneous breaking of symmetry during the phase transition known as the Anderson Higg's mechanism [43].

## 2.2.2 BCS theory

**Cooper pairs and the Cooper instability**

Cooper was able to show that an arbitrary weak but finite attractive interaction between electrons can lead to a bound state of at least one pair of electrons with an energy below the Fermi level [61]. In most cases, this weak attractive interaction is mediated by phonons, i.e. due to the interaction of the electrons with the positive ion lattice of the superconducting material. To show how this bound state is formed, we start with an operator $\Lambda^\dagger$ that adds two electrons $c_\sigma^\dagger(\mathbf{x})$ with opposite spin and zero total momentum to the system[43]:

$$\Lambda^\dagger = \int d^3x \, d^3x' \phi(\mathbf{x} - \mathbf{x}') c_\downarrow^\dagger(\mathbf{x}) c_\uparrow^\dagger(\mathbf{x}'), \tag{2.1}$$

where $\phi(\mathbf{x})$ defines the spatial distribution of the electron pair. These pairs of electrons are commonly known as Cooper pairs. It might not be clear at the first glance that this operator adds an electron pair with zero net momentum to the system but by transforming the fields into momentum space, using $c_\sigma^\dagger(\mathbf{x}) = \frac{1}{\sqrt{V}} \sum_\mathbf{k} c_{\mathbf{k}\sigma}^\dagger e^{-i\mathbf{k}\mathbf{x}}$ (where $V$ denotes the volume of the system), this fact becomes more apparent:

$$\Lambda^\dagger = \sum_\mathbf{k} \phi_\mathbf{k} c_{\mathbf{k}\downarrow}^\dagger c_{-\mathbf{k}\uparrow}^\dagger. \tag{2.2}$$

The amplitude $\phi_\mathbf{k}$ defines properties of the electron pair and furthermore the characteristics of the resulting superconductor. It can be obtained by:

$$\phi_\mathbf{k} = \int d^3x e^{-i\mathbf{k}\mathbf{x}} \phi(\mathbf{x}). \tag{2.3}$$

Therefore, the pair operator can be written as a sum of Cooper pairs that are weighted by $\phi_\mathbf{k}$ and have opposite momenta $\mathbf{k}$. In the original work of BCS, $\phi_\mathbf{k}$ was considered to be isotropic ($\phi_\mathbf{k} \propto f(|\mathbf{k}|)$) [60], which is the case for a large range of conventional superconductors with different crystal symmetries and, therefore, shows that this assumption is well-founded. This kind of superconductivity is called *s*-wave, following the naming style of the isotropic *s* atomic orbital.

The wave function of the Cooper pair in momentum space has the following form:

$$|\Psi_0\rangle = \Lambda^\dagger |\text{FS}\rangle = \sum_{|\mathbf{k}|>k_F} \phi_\mathbf{k} |\mathbf{k}_P\rangle, \tag{2.4}$$

where $|\text{FS}\rangle = \prod_{|\mathbf{k}|<k_F} c_{\mathbf{k}\downarrow}^\dagger c_{-\mathbf{k}\uparrow}^\dagger |0\rangle$ denotes the filled Fermi sea, $k_F$ the Fermi momentum and $|\mathbf{k}_P\rangle$ a single pair wave function.

We suppose that the Hamiltonian of the superconductor can be written as:

$$H = \sum_{\mathbf{k}\sigma} \epsilon_\mathbf{k} c_{\mathbf{k}\sigma}^\dagger c_{\mathbf{k}\sigma} + \hat{V}, \tag{2.5}$$

where $\epsilon_\mathbf{k}$ is the single particle dispersion relationship, describing the interactions of the electrons with the lattice of the material and neatly hiding the underlying physics. $\hat{V}$ describes the attractive interaction between two electrons. It is further assumed that the repulsive Coulomb interaction is screened out sufficiently by the positive ions in the lattice so that it is negligible compared to the attractive interaction.

Applying the Hamiltonian to the pair wave function yields:

$$H |\Psi_0\rangle = 2 \sum_{|\mathbf{k}|>k_F} \epsilon_\mathbf{k} \phi_\mathbf{k} |\mathbf{k}_P\rangle + \sum_{|\mathbf{k}|,|\mathbf{k}'|>k_F} V_{\mathbf{k}\mathbf{k}'} \phi_{\mathbf{k}'} |\mathbf{k}_P\rangle, \tag{2.6}$$

with $V_{\mathbf{k}\mathbf{k}'} = \langle \mathbf{k}_P| \hat{V} |\mathbf{k}_P\rangle$ describing a two particle scattering amplitude. The scattering amplitude gives the probability for a bound Cooper pair, consisting of two electrons with the momenta $\mathbf{k}$ and $-\mathbf{k}$, to scatter into a pair with momenta $\mathbf{k}'$ and $-\mathbf{k}'$. This process can be described by the Feynman diagram shown in Figure 2.1 and illustrates that a scattering process for such an interaction does not lead to a loss in net momentum for the electron pair, as compared to a single electron scattering process which can lead to resistive losses in normal materials. Typically, $V_{\mathbf{k}\mathbf{k}'}$ depends only weakly on momentum and is attractive within a small energy region around the Fermi surface [61]. This motivated Cooper to simplify the scattering amplitude $V_{\mathbf{k}\mathbf{k}'}$ to [43, 46, 61]:

$$V_{\mathbf{k}\mathbf{k}'} = \begin{cases} -\frac{g_0}{V} & \text{if } |\epsilon_\mathbf{k}|, |\epsilon_{\mathbf{k}'}| < \omega_D \\ 0 & \text{otherwise.} \end{cases} \tag{2.7}$$
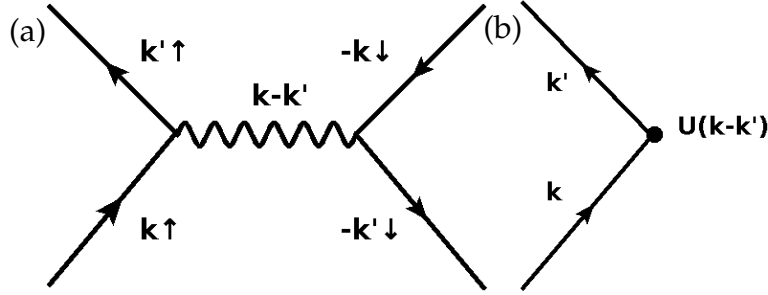
Figure 2.1: (a) Feynman diagram for a phonon mediated electron-electron interaction. The incoming electron on the left excites a phonon by scattering and loses the momentum $\mathbf{k}' - \mathbf{k}$. The phonon transfers this momentum to the other electron of the Cooper pair, leading to zero net momentum loss throughout the whole process. (b) In contrast to that, there is an effective momentum loss in a single electron scattering process which leads to electric resistivity in non-superconducting materials.

$\omega_D$ defines the cut-off energy of the interaction and $g_0$ is a constant coupling strength between an electron pair. Note that $\epsilon_{\mathbf{k}}$ is defined to be zero at the Fermi surface.

This approximation allows us to solve the Schrödinger equation of this problem by identifying $|\Psi_0\rangle$ to be an eigenstate of the Hamiltonian. The energy of the Cooper pair is then given by [43, 46]:

$$E = -2\omega_D e^{-\frac{2}{g_0 N(0)}}, \tag{2.8}$$

with $N(0)$ being the density of states at the Fermi level.

As long as $g_0$ is finite, the energy of the Cooper pair will be below the Fermi energy and, therefore, the state $|\Psi_0\rangle$ is a bound state. What is particular about this state is that the pair has a total spin of zero. Thus, the pair operator describes a boson and the Cooper pairs, underlying the bosonic commutation relationship, do not abide the Fermi exclusion principle. This allows the pairs to condense macroscopically, similar to a Bose-Einstein-condensate.

Another interesting feature of Eqn. 2.8 is that it diverges around $g_0 = 0$, preventing a perturbative treatment of this theory. This might have contributed greatly to the delay of developing a successful treatment of superconductivity [46]. It also prohibits single particle scattering within the

theory, which would arise in such a perturbation theory. Single particle scattering gives rise to electrical resistance in a normal material since electrons lose momentum during scatter events (see Fig. 2.1(b)), and the lack thereof is the reason for the zero resistance in superconductivity.

**The BCS Hamiltonian and the BCS wave function**

Following Cooper's idea that an arbitrary weak attractive interaction can lead to a bound state within the superconductor (Sec. 2.2.2), BCS proposed the following model Hamiltonian [60]:

$$H_{BCS} = \sum_{\mathbf{k}\sigma} \epsilon_{\mathbf{k}\sigma} c^\dagger_{\mathbf{k}\sigma} c_{\mathbf{k}\sigma} + \sum_{\mathbf{k}\mathbf{k}'} V_{\mathbf{k}\mathbf{k}'} c^\dagger_{\mathbf{k}\uparrow} c^\dagger_{-\mathbf{k}\downarrow} c_{-\mathbf{k}'\downarrow} c_{\mathbf{k}'\uparrow}. \tag{2.9}$$

The first term in this Hamiltonian describes the kinetic energy of the single electrons and the second term the electron-electron interactions that eventually lead to the superconducting behaviour of the material. The interaction strength $V_{\mathbf{k}\mathbf{k}'}$ can come in many varieties but in its simplest form, the conventional $s$-wave superconductor, $V_{\mathbf{k}\mathbf{k}'}$ is isotropic and constant within a small energy band around the Fermi surface (2.7) [43].

As a candidate wave function for the ground state, BCS used a coherent state of the Cooper pair operator [43]:[2]

$$|\Psi_{BCS}\rangle = e^{\Lambda^\dagger} |0\rangle = \prod_{\mathbf{k}} e^{\phi_{\mathbf{k}} c^\dagger_{\mathbf{k}\downarrow} c^\dagger_{-\mathbf{k}\uparrow}} |0\rangle = \prod_{\mathbf{k}} \left(1 + \phi_{\mathbf{k}} c^\dagger_{\mathbf{k}\downarrow} c^\dagger_{-\mathbf{k}\uparrow}\right) |0\rangle \tag{2.10}$$

In the last step, the exponential function was expanded and quadratic or terms of higher order were disregarded due to the Pauli exclusion principle ($(c^\dagger_{\mathbf{k}\sigma})^n |0\rangle = 0$ for $n > 1$).

Using this wave function, BCS was able to calculate many properties of conventional superconductors by applying a variational approach such as the superconducting gap, the critical magnetic field strength, the specific heat capacity and many more [60].

However, we will follow a different approach within this work that is more suitable for our purposes, namely the mean field approximation.

---

[2] The real ground state is a $N$-electron wave function $|BCS\rangle = \sum g(k_i, \ldots, k_l) c^\dagger_{\mathbf{k}_i\downarrow} c^\dagger_{-\mathbf{k}_i\uparrow} \cdots c^\dagger_{\mathbf{k}_l\downarrow} c^\dagger_{-\mathbf{k}_l\uparrow} |0\rangle$ [46] which weights all possible combinations of the $N/2$ Copper pairs with $g(k_i, \ldots, k_l)$. However, this approach was deemed infeasible due to the tremendous amount of coefficients needed.

### 2.2.3 Mean field description

Applying a mean field approximation to the BCS theory yields a quadratic Hamiltonian (2.9), which can be written down in a matrix form and used in a tight binding model.

At the critical temperature $T_C$, the superconductor undergoes a phase transition. This phase transition marks the emergence of a macroscopic condensate of Cooper pairs in the system. In other words, the expectation value of the pair operator $\langle F_{\mathbf{k}} \rangle = \langle c_{-\mathbf{k}\downarrow} c_{\mathbf{k}\uparrow} \rangle$ becomes extensive in volume[3]. The occupation strength of this phase can be characterised by the superconducting order parameter $\Delta$:

$$\Delta = |\Delta| \, \mathrm{e}^{i\phi} = -\frac{g_0}{V} \sum_{|\epsilon_{\mathbf{k}}| < \omega_D} \langle F_{\mathbf{k}} \rangle. \tag{2.11}$$

It is an intensive variable with an amplitude and phase[4]. $\Delta$ can be seen as a measure for the robustness of the superconducting state and defines the superconducting band gap which will be discussed in Section 2.2.4 below).

By inserting the expectation value of $F_{\mathbf{k}}$ in the interaction part of the $s$-wave BCS Hamiltonian,

$$H_{BCS,int} = -\frac{g_0}{V} \sum_{|\epsilon_{\mathbf{k}}|, |\epsilon_{\mathbf{k}'}| < \omega_D} c_{\mathbf{k}\uparrow}^{\dagger} c_{-\mathbf{k}\downarrow}^{\dagger} c_{-\mathbf{k}'\downarrow} c_{\mathbf{k}'\uparrow}$$

$$= -\frac{g_0}{V} \sum_{|\epsilon_{\mathbf{k}}|, |\epsilon_{\mathbf{k}'}| < \omega_D} \left( \langle F_{\mathbf{k}}^* \rangle + c_{\mathbf{k}\uparrow}^{\dagger} c_{-\mathbf{k}\downarrow}^{\dagger} - \langle F_{\mathbf{k}}^* \rangle \right) \left( \langle F_{\mathbf{k}'} \rangle + c_{-\mathbf{k}'\downarrow} c_{\mathbf{k}'\uparrow} - \langle F_{\mathbf{k}'} \rangle \right).$$
$$\tag{2.12}$$

The Hamiltonian can be rewritten in terms of the fluctuations $\delta F_{\mathbf{k}} =$

---

[3]Note that removing one pair $c_{-\mathbf{k}\downarrow} c_{\mathbf{k}\uparrow}$ from the Fermi sphere describes the creation of a Cooper pair.

[4]$\Delta$ can be complex valued since $F_{\mathbf{k}}$ is not a hermitian operator.

$F_{\mathbf{k}} - \langle F_{\mathbf{k}} \rangle$ and $\Delta$:

$$H_{BCS,int} = -\frac{g_0}{V} \sum_{|\epsilon_{\mathbf{k}}|, |\epsilon_{\mathbf{k}'}| < \omega_D} \left( \langle F_{\mathbf{k}}^* \rangle + \delta F_{\mathbf{k}}^* \right) \left( \langle F_{\mathbf{k}'} \rangle + \delta F_{\mathbf{k}'} \right)$$

$$= \frac{V}{g_0} \Delta^* \Delta + \sum_{|\epsilon_{\mathbf{k}}| < \omega_D} \left( \Delta^* F_{\mathbf{k}} + F_{\mathbf{k}}^* \Delta \right) - \frac{g_0}{V} \sum_{|\epsilon_{\mathbf{k}}|, |\epsilon_{\mathbf{k}'}| < \omega_D} \delta F_{\mathbf{k}}^* \delta F_{\mathbf{k}'}.$$

$$(2.13)$$

In the thermodynamic limit of $V \to \infty$, the quadratic term in the fluctuations becomes negligible [43]. The quadratic term in $\Delta$ results only in a constant shift in energy and does not contribute to the dynamics of the system. Therefore, this term can be discarded for simplicity since we are only interested in relative energies. The resulting total mean field Hamiltonian for superconductivity takes on the following form:

$$H_{MF} = \sum_{\mathbf{k}\sigma} \epsilon_{\mathbf{k}\sigma} c_{\mathbf{k}\sigma}^\dagger c_{\mathbf{k}\sigma} + \sum_{|\epsilon_{\mathbf{k}}| < \omega_D} \left( \Delta^* c_{-\mathbf{k}\downarrow} c_{\mathbf{k}\uparrow} + c_{\mathbf{k}\uparrow}^\dagger c_{-\mathbf{k}\downarrow}^\dagger \Delta \right) \qquad (2.14)$$

The first term in the interaction term can be interpreted as annihilating a pair of electrons $c_{-\mathbf{k}\downarrow} c_{\mathbf{k}\uparrow}$ and creating a Cooper pair $\Delta^*$ in the condensate whereas the second term, the hermitian conjugate, is the reverse process, a Cooper pair scattering into two fermions. This Hamiltonian does not conserve the number of fermions in the system[5] and, therefore, it has to be treated as a grand canonical ensemble.

### 2.2.4 The Bogoliubov transformation

**Nambu spinor basis**

The mean field treatment of the BCS Hamiltonian (2.9) transformed it into a quadratic form (2.14). By using the Nambu spinor basis [63, 64] and the

---

[5]This is opposed to the BCS Hamiltonian (2.9). This effect is caused from breaking the local U(1) symmetry with the mean field approximation, meaning that the Hamiltonian is not invariant under the transformation $c \to c\, e^{i\varphi(x)}$ (where $\varphi(x)$ is an arbitrary local phase). Since the U(1) symmetry is related to the conservation of particles by Noether's theorem [62], the symmetry breaking leads to the loss of a fixed number of particles in the system.

Bogoliubov transformation [65], it is now possible to diagonalise the mean field Hamiltonian.

The Nambu spinor $\psi_\mathbf{k}$, named after the electron spinor field in quantum field theory, combines electrons $c_{\mathbf{k}\uparrow}^\dagger$ and holes $c_{-\mathbf{k}\downarrow}$ in one basis and is defined as:

$$\psi_\mathbf{k} = \begin{pmatrix} c_{\mathbf{k}\uparrow} \\ c_{-\mathbf{k}\downarrow}^\dagger \end{pmatrix}, \tag{2.15}$$

and its hermitian conjugate is:

$$\psi_\mathbf{k}^\dagger = \begin{pmatrix} c_{\mathbf{k}\uparrow}^\dagger, & c_{-\mathbf{k}\downarrow} \end{pmatrix}. \tag{2.16}$$

These spinors are subjected to the fermionic commutator algebra:

$$\{\psi_\mathbf{k}, \psi_{\mathbf{k}'}^\dagger\} = \delta_{\mathbf{k},\mathbf{k}'} \tag{2.17}$$

Using the Nambu spinors as a basis, the Hamiltonian can be written in the following compact form [26, 43][6]:

$$H_{MF} = \sum_\mathbf{k} \psi_\mathbf{k}^\dagger \begin{bmatrix} \epsilon_\mathbf{k} & \Delta \\ \Delta^* & -\epsilon_{-\mathbf{k}} \end{bmatrix} \psi_\mathbf{k} = \sum_\mathbf{k} \psi_\mathbf{k}^\dagger \underline{h}_\mathbf{k} \psi_\mathbf{k}, \tag{2.18}$$

where $-\epsilon_{-\mathbf{k}}$ is the energy dispersion relationship of a hole $c_{-\mathbf{k}\sigma}$ and $\underline{h}_\mathbf{k}$ denotes the so called Nambu matrix. This formalism is known as the Bogoliubov-de Gennes (BdG) formalism.

Assuming that $\epsilon_\mathbf{k}$ is even in $\mathbf{k}$, the eigenvalues of this matrix are [43]:

$$E_\mathbf{k} = \pm\sqrt{\epsilon_\mathbf{k}^2 + |\Delta|^2}, \tag{2.19}$$

and its corresponding eigenvectors are:

$$\begin{pmatrix} u_\mathbf{k} \\ v_\mathbf{k} \end{pmatrix} \quad \text{and} \quad \begin{pmatrix} -v_\mathbf{k}^* \\ u_\mathbf{k}^* \end{pmatrix}. \tag{2.20}$$

The eigenstates are a mixture of electrons and holes with a share of $u_\mathbf{k}$ and $v_\mathbf{k}$, respectively. The dispersion relationship (2.19) and how it

---

[6]One way to arrive from Eqn. (2.14) at Eqn. (2.18) is to expand the sum in the kinetic Hamiltonian in terms of up and down spins, commute down spin operators and, finally, relabel their momenta $\mathbf{k} \to -\mathbf{k}$. The resulting constant term $\sum_\mathbf{k} \epsilon_\mathbf{k}$ was neglected.

combines electrons and holes is illustrated in Fig. 2.2 by comparing it to an interaction free continuum dispersion relationship. Note that a finite value of $\Delta$ will always lead to a gap opening in the band structure, whose implications will be discussed more comprehensively after the diagonalisation of the Hamiltonian below.
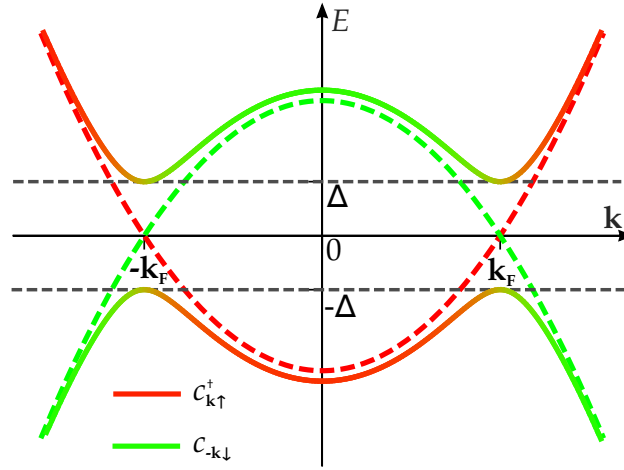


Figure 2.2: Dispersion relationship of a model superconductor. The dashed red and green lines show the dispersion of a continuum model for electrons $c^\dagger_{\mathbf{k}\uparrow}$ and holes $c_{-\mathbf{k}\downarrow}$, respectively. A finite order parameter $\Delta$ in the system leads to a mixing of electron and hole states and opens a gap in the band structure of size $2\Delta$ (solid lines). The mixture of colours along the solid lines is proportional to the amount of electron (red) and hole (green) states at each $\mathbf{k}$. Adapted from reference [43].

**Diagonalisation of the Nambu Hamiltonian**

The Hamiltonian (2.18) can be diagonalised by introducing so called Bogoliubov quasiparticles $a^\dagger_{\mathbf{k}\uparrow}$ [65] which are mixtures of electron and hole states:

$$a^\dagger_{\mathbf{k}\uparrow} = c^\dagger_{\mathbf{k}\uparrow} u_{\mathbf{k}} + c_{-\mathbf{k}\downarrow} v_{\mathbf{k}}$$
$$a_{-\mathbf{k}\downarrow} = c_{-\mathbf{k}\downarrow} u^*_{\mathbf{k}} - c^\dagger_{\mathbf{k}\uparrow} v^*_{\mathbf{k}}$$

$$(2.21)$$

By writing the Hamiltonian in terms of these quasiparticles, a diagonalised form of the Hamiltonian is obtained.

$$H_{Bogoliubov} = \sum_{\mathbf{k}} E_{\mathbf{k}} \left( a_{\mathbf{k}\uparrow}^{\dagger} a_{\mathbf{k}\uparrow} + a_{-\mathbf{k}\downarrow}^{\dagger} a_{-\mathbf{k}\downarrow} \right) \tag{2.22}$$

The quasiparticle density of states obtained through this diagonalisation is shown in Figure 2.3. Due to the superconducting interaction, the density of states is gapped around the Fermi level at $E = 0$ by $2\Delta$ and similar to a density of states of an insulator. This may seem paradox at first glance since the superconductor shows perfect conductivity in high contrast to an insulator. However, this can be explained by the fact that in a material the electrons which are excited into the conduction band are responsible for electrical charge transport. In a superconductor, on the other hand, the conduction is due to the Cooper pairs which already exist in the ground state of the material.
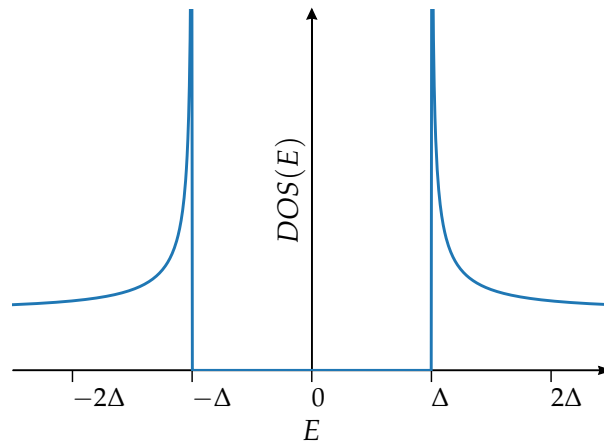


Figure 2.3: Bogoliubov quasiparticle density of states for a BCS superconductor [43]. Note that the density of states is gapped around the Fermi level at $E = 0$ by $2\Delta$.

## 2.3 Majorana fermions

Fermions in general are particles with half integer spins and obey the Fermi statistics, i.e. their creation and annihilation operators anticommute. In quantum field theory, they are defined as the solution of the Dirac equation, which resulted from formulating Schrödinger's equation in terms of relativistic fields [66]. Dirac's solution to this equation utilises complex fields to describe fermions. This complex solution proved to be applicable to all known fermions, except for the neutrino whose classification is still unknown [2]. Majorana, on the other hand, was able to find a real field solution for Dirac's equation [1]. This solution implied that particles described by it would be their own antiparticles, i.e. Majorana particles and antiparticles are the same. As of today, there is no experimental proof that Majorana fermions exist but there are theories assuming that the neutrinos are Majorana-like [3, 4]. Other theorised particles arising from supersymmetry which are suspected to be Majorana particles as well [2].

In condensed matter physics, on the other hand, the definition for Majorana fermions $\gamma^\dagger$ is that they are fermionic quasiparticles which are their own antiparticles [2]. In the language of second quantisation, this can be formulated as $\gamma^\dagger = \gamma$.

A simple example for quasiparticles which are their own antiparticles is:

$$\gamma^\dagger = c_i^\dagger c_j + c_i c_j^\dagger. \tag{2.23}$$

In this case, $\gamma$ describes a mixture of holes and electrons on different sites $i$ and $j$. However, quasiparticles of this kind are bosonic since they commute rather than anticommute like fermions and, therefore, do not qualify as Majorana fermions. The Bogoliubov quasiparticles $a_{\mathbf{k}\uparrow}^\dagger$ occurring in conventional $s$-wave superconductors (Sec. 2.2.4), are fermions but they are not their own quasiparticles $a_{\mathbf{k}\uparrow}^\dagger \neq a_{\mathbf{k}\uparrow}$.

In order to achieve Majorana fermions in conventional superconductors, one must look at more exotic systems. For example, there are material combinations hosting Dirac-like quasiparticles, e.g. electrons with an energy dispersion similar to the Dirac equation. This Dirac-like dispersion relationship is predicted to occur in topological insulators and superconductors [10, 26, 35, 36, 50–52, 67–69]. Therefore, we will discuss how one can construct a system with a Dirac energy dispersion in Section 2.4 below

and then explain how it can occur in superconductors and how it can be used to create Majorana fermions.

## 2.4 Topological band structures

This section deals with the introduction of topology in general and its application to the concept of band structures. We will further discuss how band structures with different topologies can lead to a Dirac-like energy dispersion relationship which is an important component for creating Majorana fermions in a topological superconductor.

### 2.4.1 Topology
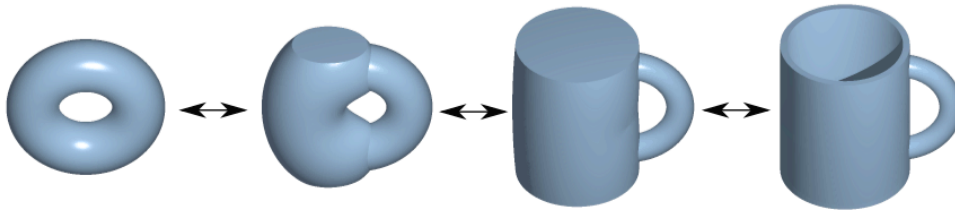


Figure 2.4: Continuous transformation of a torus into a mug. Note that the number of holes in the object stays invariant during the whole process. Source: Original pictures by Lucas V. Barbosa [70]

In general, topology is a branch of mathematics studying properties of spatial manifolds which stay invariant under continuous transformations. One of these properties could be the number of holes in a manifold. For example, it is possible to transform a torus (or doughnut) shaped object into a mug shape only by using continuous transformations like stretching and compressing as illustrated in Fig. 2.4. This means that these two objects belong to the same topological class or, in more radical terms, they are the same from a topological point of view. On the other hand, it is not possible to transform a torus into a sphere without merging or gluing surfaces together. This process of gluing is a discontinuous transformation and reduces the number of holes in the manifold by one. The same applies

to converting a torus into a double torus, which requires the process of cutting a new hole into the object making it again a discontinuous transformation. Thus, cutting and gluing are processes that change the number of holes and, therefore, the topology of the objects (Fig. 2.5).
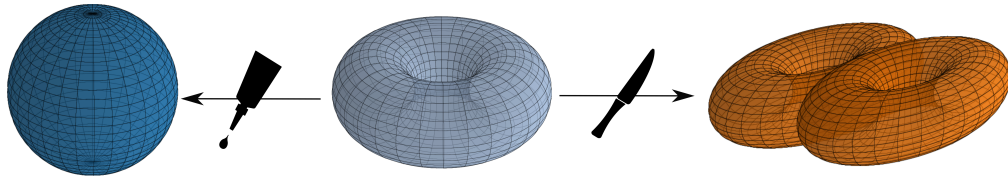


Figure 2.5: Examples for discontinuous transformations. In order to go from a torus (middle) to a sphere (left), the surface has to be glued at one point of the transformation to close the hole in the middle. For a transformation from a torus to a double torus (right), a cut is necessary to create the second hole. Both transformations do not conserve the number of holes and, therefore, change the topology of the object.

**Differential geometry**

Before we explain the concept of topological invariants in solid state physics, we will have a look at some important concepts of differential geometry. Having understood these concepts, we will move on to introducing a topological invariant for band structures, the so called first Chern number.

Usually, geometry is associated with the two- or three-dimensional Euclidean space. In order to demonstrate other geometrical spaces, we will start by thinking of a piece of paper lying on a flat surface representing the two-dimensional Euclidean space. Known concepts of Euclidean space apply here. For example, measuring a distance between points can be done easily by drawing a straight line between them and measuring its length. This particular way of measuring the distance is also known as Euclidean metric and the straight line between two points can be seen as a connection, which is a rule that defines how to connect points in space.

However, what would happen if the piece of paper was not lying on a flat surface but was embedded in the surface of a sphere[7]? Measuring the

---

[7]In this context, it is not meant that the piece of paper becomes a curved three-

distance between two points might again seem straightforward. It can be done by connecting the two points with a straight line along the curvature of the sphere and measuring its length. However, we should to take care here and have a more rigorous look at what it means to connect two points with a straight line on a bent geometry.
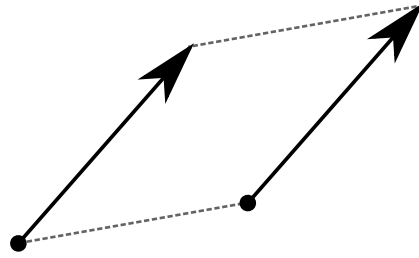


Figure 2.6: Parallel transport of a vector in Euclidean space.

In order to be able to define connecting two points accurately, we will first introduce the concept of parallel transport. It describes the process of moving the base point of a vector from one point in space to another, while keeping the orientation of the vector the same. In Euclidean space, parallel transport is simply realised by parallel shifting the vector from one base point to another (Fig. 2.6). In the case of a sphere, this procedure is slightly more complicated. First of all, a vector on the surface of a sphere is defined on a tangent plane spanned through the base point of the vector. The vector can be transported by moving its base point by infinitesimal small steps along the surface and with each step, the vector will be projected into its new tangent plane. This projection is described by a so called connection. To use graphical terms, imagine standing on a sphere big enough so you cannot perceive its curvature and holding an arrow parallel to the ground representing the vector. If you now start moving on the surface, while keeping the arrow pointing in the same direction and parallel to the ground, the arrow (vector) is parallel transported along the surface. The difference to Euclidean parallel transport becomes quite clear when, for example, a vector pointing north is parallel transported from the equator to a pole (red vectors in Fig. 2.7). From the point of view of an observer

---

dimensional object, it rather still represents a two-dimensional plane, but with a different geometry as compared to a flat piece of paper.

on the surface of the sphere, the vector is always pointing in the same direction and only changes its location but, from the outside, the vector is first pointing upwards and after the transport it is parallel to the tangent plane at the pole.

To come back to the problem of drawing a straight line on a sphere, it can be accomplished by making infinitesimal steps in the direction of the vector and parallel transporting it at the same time according to a connection defined for the sphere.
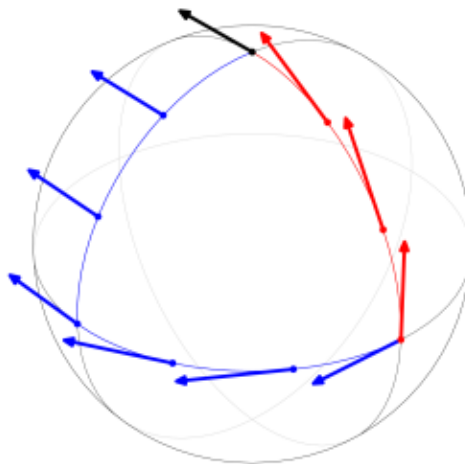


Figure 2.7: Parallel transport of a vector along the surface. The basis point of the red vector is parallel transported from a point on the equator to the north pole (black vector). From there the loop to the starting point is closed by following a different path (blue vector), resulting in another orientation of the vector at the initial position of the basis point. Source: Picture by Florian Jung [71].

Another interesting feature about the surface of a sphere (and of many other geometrical objects) compared to the Euclidean plane is that if you parallel transport a vector along a loop, it can change its orientation. For example, starting again at the equator with a vector pointing north and parallel transporting it to the north pole, then moving 90° from the original direction east to the equator. Eventually, by closing the loop by following the equator eastwards, the vector will point to the west, i.e. it is rotated by 90° compared to the original orientation (Fig. 2.7). This phenomenon of change in the direction of vectors which were parallel transported along

a loop is known as curvature[8]. The Euclidean plane, for example, has a constant curvature of zero, since there is no arbitrary closed loop which would change the orientation of a vector.

From the curvature of a surface, topological information about the object itself can be extracted, e.g. the number of holes in the object can be related to the integral over the curvature of a closed object. This relation is known as the Euler characteristic [72].

**The first Chern number**

The first Chern number can be used as a powerful tool for distinguishing different topological phases of band structures. In order to arrive at an expression for this topological invariant and to understand what is meant by a topological phase, we will employ the concepts of a connection and curvature to Hamiltonians describing band structures.

First, we begin with defining a connection for a Hamiltonian in $\mathbf{k}$-space, starting with a $n \times n$ sized Hamiltonian $H(\mathbf{k})$ in two $\mathbf{k}$-dimensions. Initially, we assume $H(\mathbf{k})$ to be non-degenerate for all values of $\mathbf{k}$. In comparison to the sphere, the coordinates on the surface of the sphere are substituted by the $\mathbf{k}$-space coordinates $k_x$ and $k_y$[9]. As vectors on the sphere were defined in the tangential plane of the point, the vectors associated with each point of $(k_x, k_y)$ on the Hamiltonian are the corresponding eigenvectors $\left| \Psi^{(\lambda)}(k_x, k_y) \right\rangle$. We will now introduce a connection for this Hamiltonian describing the change of the eigenvectors when moving through $\mathbf{k}$-space. Strictly speaking there are $n$ eigenvectors at each $\mathbf{k}$-point and therefore, $n$ different connections. In order to keep track of the eigenvectors in an unambiguous way, they are sorted by their respective energy eigenvalues in increasing order and are assigned an index $\lambda$ (you could also think of counting through the energies of the bands at one particular $\mathbf{k}$-point from bottom to top). For example, $\left| \Psi^{(0)}(k_x, k_y) \right\rangle$ is the eigenvector of the lowest energy eigenstates at the point $(k_x, k_y)$ and the

---

[8]The curvature is defined as the change of direction of a vector transported along an infinitesimally long loop.

[9]Strictly speaking, this picture should not be taken literally. In practice, the k-coordinates would usually be mapped to the surface of a torus if periodic boundary conditions are used.

parallel transport of this eigenvector to any point $(k'_x, k'_y)$ is described by the $0^{\text{th}}$ connection. The connection describing the change of each $\lambda^{\text{th}}$ eigenvector is known as the Berry connection [73]. In formulas, the Berry connection $A_\mu^{(\lambda)}$ can be specified as:

$$A_\mu^{(\lambda)} = - \operatorname{Im} \left( \left\langle \Psi^{(\lambda)} \middle| \partial_\mu \Psi^{(\lambda)} \right\rangle \right).$$ (2.24)

The expression $\left\langle \Psi^{(\lambda)} \middle| \partial_\mu \Psi^{(\lambda)} \right\rangle$ can be seen as the change of the $\lambda^{\text{th}}$ eigenvector in the direction $\mu$ with respect to its original direction $\left| \Psi^{(\lambda)} \right\rangle$.

Given this connection, the so called Berry curvature of the Hamiltonian can be derived as [51]:

$$\mathcal{F}_{\mu\nu}^{(\lambda)} = \partial_\mu A_\nu^{(\lambda)} - \partial_\nu A_\mu^{(\lambda)}.$$ (2.25)

By integrating the curvature over the first Brillouin zone $S$, the first Chern number is obtained[10] [47]:

$$C_1^{(\lambda)} = \frac{i}{2\pi} \int_S \mathcal{F}_{\mu\nu}^{(\lambda)} dS.$$ (2.26)

Since the first Chern number is analogous to the Euler characteristic, one can of think of this number as the number of holes in the manifold represented by the Hamiltonian. The first Chern number is integer valued and one of its interesting features is that it is invariant under topological continuous transformations of the Hamiltonian, i.e. changing parameters without introducing degeneracies to the band structure. This requirement of the Hamiltonian to be non-degenerate allows for another interesting feature. If the Hamiltonian is degenerate at one point $(k_x, k_y)$ and at least two bands cross each other there, the whole formalism of the construction of the Berry connection breaks down. At the degeneracy, it is no longer possible to assign an unambiguous index to the crossing bands. Therefore,

---

[10]In practice, the Chern number is often calculated numerically. Since the eigenvectors are only defined up to an arbitrary phase factor (phase gauge), the calculation of the derivative in the Berry connection can be unfeasible. In this case, the Kubo formula is normally used, which is equivalent to the Chern number and does not rely on derivatives of the eigenvectors [51, 73, 74].

the Berry connection can have two or more different values at this point and it cannot be determined which value should be associated with which band. At this point $(k_x, k_y)$, the bands are able to change their Chern numbers, but this exchange is somewhat restricted, namely the sum of the Chern numbers of all crossing bands will stay invariant [35]. By using this restriction, the Chern number can be used to detect degeneracies between Hamiltonians with different parameters, i.e. if the Hamiltonians have a different Chern number for two sets of parameters there must be a degeneracy at one point in the parameter space in between.

This characteristic can be particularly useful when studying systems with a band gap around the Fermi level, such as insulators and superconductors. Special interest usually lies on finding degeneracies between the valence and the conduction band, closing the band gap for a set of parameters. In practice, a degeneracy can be detected by summing the Chern number of all bands underneath the Fermi level and then comparing this sum between different states of the Hamiltonian. If the sum has changed, there must have been a gap closing between those two states. This closing of the band gap can be interpreted in topological terms as the process of cutting a hole in a sphere (represented by one phase of the Hamiltonian) and consequently transforming it into a torus (Fig. 2.5). Parameter regimes with different topologies are usually called topological phases.

We will make use of this tool in the next Section when we look at a certain toy model for topological insulators.

## 2.4.2 Topological insulators

We will start our introduction to topological band structures with topological insulators, because their band structures are simpler than those of topological superconductors since they allow to use a toy model that ignores the spin of electrons. After establishing the topological concepts for band structures, we will add superconductivity to the model and show an example of a *s*-wave superconductor system which hosts Majorana fermions.

A simple model for an insulator can be realised by two parabolic bands
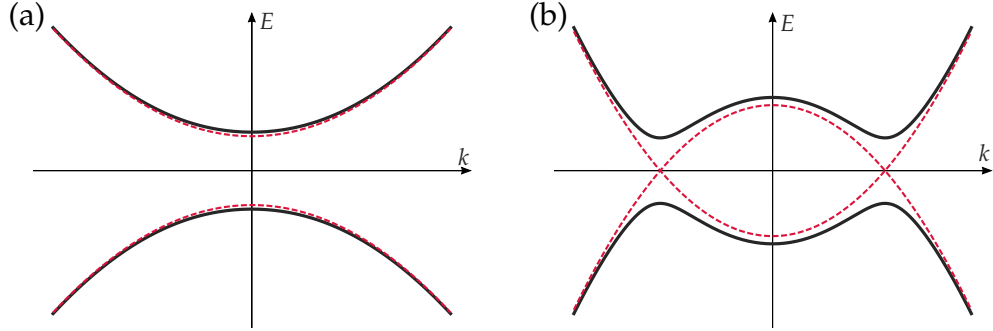
Figure 2.8: Dispersion relationship of a simple insulator (dashed red lines) and with an additional Rashba spin-orbit interaction (black lines).(a) $M > 0$ Case of a positive mass gap (b) $M < 0$ Band inversion with negative mass gap.

with a band gap of $2M$ at $\mathbf{k} = 0$:

$$H = \begin{bmatrix} \epsilon & 0 \\ 0 & -\epsilon \end{bmatrix}, \tag{2.27}$$

with $\epsilon$ in this case defined as:

$$\epsilon = \mathbf{k}^2 + M \tag{2.28}$$

The dispersion relationship of this simple model is shown in Fig. 2.8 as red dashed lines. An important role in the classification of the topological phase of the band structure is constituted by the mass gap $M$ that is half the value of the band gap at $\mathbf{k} = 0$[11]. For $M > 0$, the model describes a direct insulator with an energy gap of $2|M|$ but in the case of band inversion, i.e. a negative mass gap $M < 0$, the model describes a metallic dispersion relationship with no band gap and degeneracies at $|\mathbf{k}| = \sqrt{M}$.

These degeneracies can be lifted and the band gap reopened by introducing an interaction $\Lambda$ between the two bands:

$$H = \begin{bmatrix} \epsilon & \Lambda \\ \Lambda^* & -\epsilon \end{bmatrix}. \tag{2.29}$$

---

[11]The term mass gap is borrowed from the terminology of high energy physics, where the mass gap refers to the minimal amount of energy needed to create a particle from the vacuum. In our case, it is the energy needed to create a particle either in the conduction band or a hole in the valence band, at zero momentum.

$\Lambda$ now leads to a hybridisation between the two bands if they come close to each other in energy and contributes to the following dispersion relationship:

$$E = \pm\sqrt{\epsilon^2 + |\Lambda|^2}. \tag{2.30}$$

As long as $\Lambda$ is independent of $\mathbf{k}$ and finite, the hybridisation guarantees a band gap of at least $2\,|\Lambda|$. Note that the dispersion relationship (2.30) is the same as for the $s$-wave superconductor from Section 2.2.4, with $\Delta = \Lambda$.

### 2.4.3 Rashba spin orbit coupling
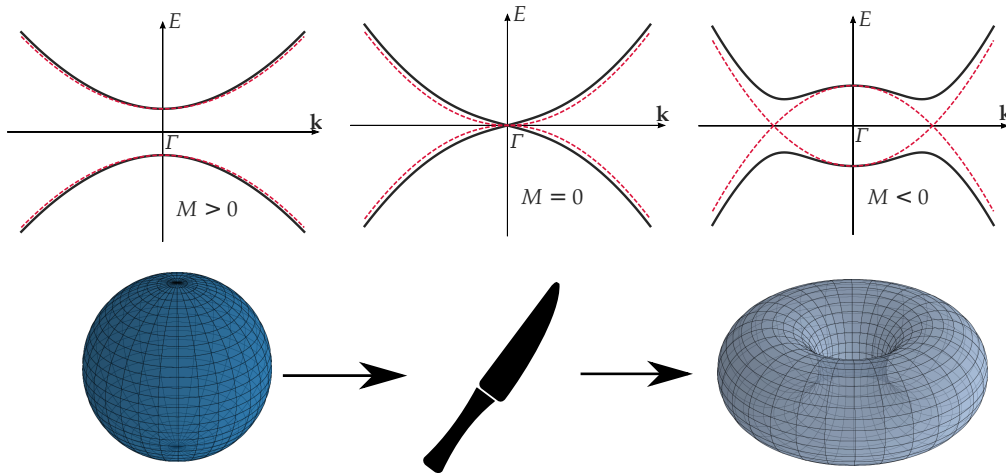


Figure 2.9: Band structures according to the dispersion relationship (2.32) for three different values of $M$. The degeneracy at $M = 0$ and $\mathbf{k} = 0$ separates the topological trivial phase $M > 0$ from the non-trivial $M < 0$ and can be compared to the process of cutting a hole in the topology of the system, analogous to the transformation of a sphere into a torus.

We will now look at a special case where $\Lambda$ is a function of $\mathbf{k}$ and reintroduce the possibility of having a degeneracy in the band structure for a special value of $M$. This degeneracy will give rise to two different phases in the topology of the system depending on $M$. The special interaction we will investigate is the so called Rashba spin orbit coupling (SOC).

The Rashba SOC occurs in crystals that lack inversion symmetry and is a relativistic effect where the electrons experience an uniaxial electric field as a magnetic field when they travel through the crystal. This effectively couples their spin to their momentum [75].

In mathematical terms, the Rashba SOC is modelled in the following form [76]:

$$\Lambda_{SOC}(\mathbf{k}) = \alpha \left(k_y + ik_x\right), \tag{2.31}$$

where $\alpha$ is the strength of the coupling. Substituting $\Lambda$ with $\Lambda_{SOC}(\mathbf{k})$ in Eqn. (2.29) leads to the following Hamiltonian and dispersion relationship:

$$H = \begin{bmatrix} k_x^2 + k_y^2 + M & \alpha\left(k_y + ik_x\right) \\ \alpha\left(k_y - ik_x\right) & -\left(k_x^2 + k_y^2\right) - M \end{bmatrix}$$
$$E = \pm\sqrt{\alpha^2\left(k_x^2 + k_y^2\right) + \left(k_x^2 + k_y^2 + M\right)^2} \tag{2.32}$$

The dispersion relationships for $M \gg 0$, $M = 0$ and $M \ll 0$ are plotted in Figure 2.9. The two cases of $M \gg 0$ and $M \ll 0$ are similar to the dispersion relationship above with a constant $\Lambda$. Both systems are gapped in the normal and band inversion case. For $M = 0$, however, the system has a degeneracy at the $\Gamma$ point ($\mathbf{k} = 0$) since the Rashba interaction is zero and, therefore, unable to part the two bands. This degeneracy leads to a topological phase transition between the two states with a positive and a negative band gap [51]. To use an analogy to Section 2.4.1, think of the degeneracy cutting a hole in the topology of the band structure (Fig. 2.9) and changing its Chern number.

We will denote the phase of $M > 0$ as the topological trivial phase and $M < 0$ as topological non-trivial[12].

**Dirac cone**

The degeneracy at $M = 0$ does not only mark the point of a topological phase transition but the bands also form a so called Dirac cone [69]. Examining the dispersion relationship (2.32) near the $\Gamma$ point yields ($k_x, k_y \approx 0$)

---

[12]The choice of which phase is denoted trivial and which is non-trivial is often artificial. In this case, the phase with $M > 0$ is usually denoted as trivial because it connects smoothly to the atomic limit and thus, the vacuum.

[26]:

$$E|_{M=0} = \pm\sqrt{\alpha^2\left(k_x^2 + k_y^2\right) + \left(k_x^2 + k_y^2\right)^2} \approx \pm\sqrt{\alpha^2\left(k_x^2 + k_y^2\right)} = \pm\alpha|\mathbf{k}|,$$
(2.33)

which resembles the shape of a cone since the bands are linear in $|\mathbf{k}|$. For small values of $M$, the dispersion relationship still reassembles the form of a cone but with a blunted tip. Assuming $|M| \ll \alpha^2$, Eqn. (2.33) can be written as:

$$E \approx \pm\sqrt{M^2 + \alpha^2\left(k_x^2 + k_y^2\right)}.$$
(2.34)

Comparing this equation to the relativistic dispersion relationship for Dirac particles, it becomes clear that both dispersion relationships are analogous to some extent [57, 77, 78]:

$$E_{Dirac} = \pm\sqrt{m^2 + |\mathbf{k}|^2},$$
(2.35)

where $m$ denotes the mass of the particle.

### 2.4.4 The bulk-boundary correspondence

The Dirac cone that is formed by the bands at $M = 0$ will prove to be an important element in the realisation of the Majorana fermions in the wire system studied in this work. This section focuses on how it is possible to create this particular feature in the band structure of a material. Tuning the properties of a material in such a way so that the mass gap becomes exactly zero can be tedious, if not unfeasible. In particular, real materials always contain impurities and imperfections to some degree and they can potentially derange the material away from a zero mass gap.

Another way to realise a zero mass gap is to bring two different materials together, one with $M$ adjusted to $M > 0$ and another with $M < 0$[13]. The exact values of $M$ are rather insignificant and can vary to so some degrees due to impurities as long as they don't change the sign of $M$. If we now consider a path crossing through the interface of both materials,

---

[13]A special example for a "material" with a positive mass gap is a vacuum. One can think of it as a material with only a valence band and the conduction band pushed to positive infinity [35].

somewhere along this path, the sign of $M$ will change, thus guaranteeing $M$ to be zero at one point. Therefore, a Dirac cone will emerge between the two materials [26] (Fig. 2.10). This effect is known as the bulk-boundary correspondence. However, the drawback of this particular construction is the loss of one dimension since the Dirac cone appears only at the boundary.
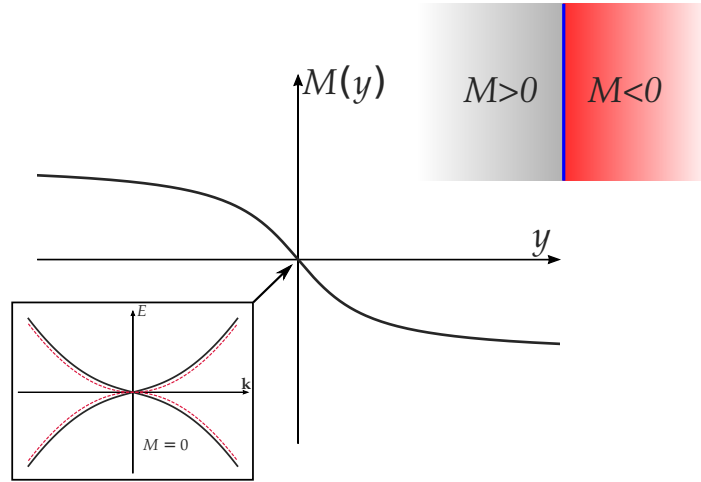


Figure 2.10: Example for the bulk-boundary correspondence. If two materials with different signed mass gaps are in contact, the value of the mass gap has to go trough zero at one point between the two materials. At this point, a Dirac cone will form in the band structure.

**Edge states**

The states that appear between the boundary of the two materials with different signs of $M$ are known as so called edge states. In order to gain some insights into the nature of these edge states, we are again interested in the low energy spectrum of the Hamiltonian, thus setting $k_x^2, k_y^2 \to 0$. Considering a two-dimensional system with a change in sign of the mass gap parameter $M$ at $y = 0$,

$$M(y) = -M \operatorname{sign}(y), \tag{2.36}$$

the Hamiltonian (2.32) can be separated into $x$ and $y$ dependent parts with the help of an inverse Fourier transformation along the $y$-axis [26]:

$$H = H_x + H_y, \tag{2.37}$$

with $H_x$ and $H_y$ defined as:

$$H_x = \begin{bmatrix} 0 & i\alpha k_x \\ -i\alpha k_x & 0 \end{bmatrix} \tag{2.38}$$

and

$$H_y = \begin{bmatrix} M(y) & -i\alpha\partial_y \\ -i\alpha\partial_y & -M(y) \end{bmatrix}. \tag{2.39}$$

The eigenstates of this Hamiltonian are provided by [26, 35, 36]:

$$\left|\Psi^{(\pm)}\right\rangle = \frac{1}{\sqrt{2}} \begin{bmatrix} 1 \\ \mp i \end{bmatrix} e^{\pm \int_0^y \frac{M(y')}{\alpha} dy'}. \tag{2.40}$$

The dispersion relationship of this state resembles a Dirac cone $E = \pm \alpha k_x$, which originates from the $x$ dependent part of the Hamiltonian since $H_y \left|\Psi^{(\pm)}\right\rangle = 0$.

The state $\left|\Psi^{(+)}\right\rangle$ with the dispersion relationship of $E = -\alpha k_x$ is located directly at the boundary. This can be seen by the fact that the integral in the exponent is always negative. Therefore, the state is decaying exponentially away from the edge. The state $\left|\Psi^{(-)}\right\rangle$, on the other hand, is an unbound state since the exponent is growing with the distance from the boundary. This means that only one branch of the Dirac cone is located at the edge.

In order to realise the other branch of the Dirac cone, we add a second boundary edge at $y = Y$ to the system so that

$$M(y) = \begin{cases} -M & \text{if } Y < y < 0 \\ M & \text{otherwise} \end{cases}. \tag{2.41}$$

Within this system, one branch of the cone will be located at $y = 0$ and the other at $y = Y$. Figure 2.11 shows a schematic of this system, the localisation of the edge states and its dispersion relationship.
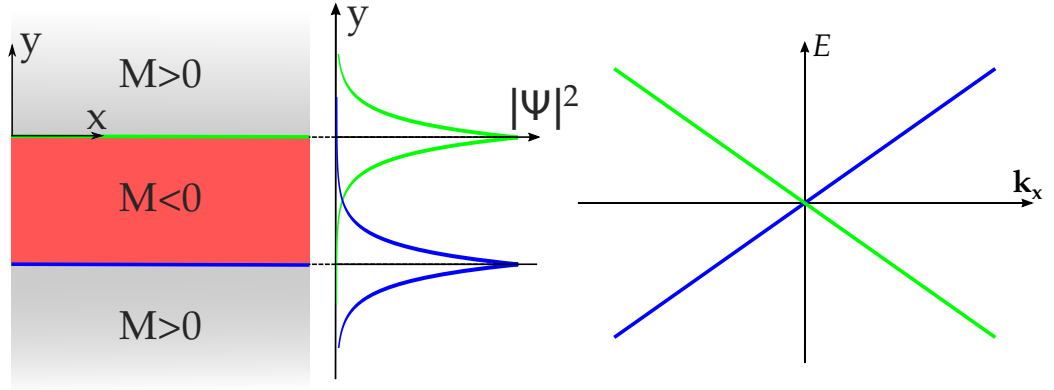
Figure 2.11: (left) Three two-dimensional stripes extending infinitely, horizontally. Their sign of $M$ is changing at each boundary. (middle) The two eigenstates of the system are either localised on the top (green) or bottom edge (blue). (right) Dirac cone like dispersion relationship. The two branches are coloured correspondingly to the edges states. Adapted from reference [26].

## 2.5 Topological superconductivity

In this section, all the previously introduced concepts of superconductivity, spin-orbit coupling and topological band structures will be combined into one system. This will give rise to a different formulation of the Bogoliubov quasiparticle that can be its own antiparticle under certain circumstances and, therefore, a Majorana fermion. Eventually, we will show how the ferromagnetic wire plays an important role in establishing those certain circumstances.

### 2.5.1 Expanding the Bogoliubov-de Gennes formalism

In order to be able to include other interactions into our model Hamiltonian, such as Rashba spin-orbit coupling, it needs to be expanded into a more general form. This can be achieved by increasing the Nambu spinor basis to four components and, therefore, doubling the Hilbert space as compared to the formulation that is described in Section 2.2.4. The Hamiltonian then has the following matrix form [25, 26, 45, 46, 65, 79]:

$$H_{BdG} = \sum_{\mathbf{k}} \psi_{\mathbf{k}}^{\dagger} \begin{bmatrix} H_{0\,\mathbf{k}} & \Delta_{\mathbf{k}} \\ \Delta_{\mathbf{k}}^{\dagger} & -H_{0\,-\mathbf{k}}^{T} \end{bmatrix} \psi_{\mathbf{k}} = \sum_{\mathbf{k}} \psi_{\mathbf{k}}^{\dagger} \underline{h}_{\mathbf{k}} \psi_{\mathbf{k}}, \tag{2.42}$$

using the basis

$$\psi_{\mathbf{k}} = \begin{pmatrix} c_{\mathbf{k}\uparrow} \\ c_{\mathbf{k}\downarrow} \\ c^{\dagger}_{-\mathbf{k}\uparrow} \\ c^{\dagger}_{-\mathbf{k}\downarrow} \end{pmatrix}. \tag{2.43}$$

$H_{0\,\mathbf{k}}$ and $\mathbf{\Delta_k}$ are two by two matrices and their exact nature will be introduced below.

The BdG formalism in this form artificially doubles the degrees of freedom in the Hamiltonian but does not add new physics to the system. Naturally, this leads to the introduction of symmetries into the system, effectively counteracting the artificial enlargement of the Hilbert space. In detail, this means that for every particle state in the BdG formalism, there is a hole state with negative energy and momentum. Therefore, since every state in the system can be linked to another one, the degrees of freedom are lowered again by half. A special characteristic of this symmetry is that it cannot be broken by physical perturbations since it is intrinsically included in the formalism. This formalism might seem pointless at first glance since it appears as if it did not yield any additional information However, it has the advantage of being able to describe various kinds of superconductivity as well as additional quadratic interactions. It also reveals an interesting characteristic of the Bogoliubov quasiparticles, as discussed in Section 2.2.4, which was concealed by the limitations of $s$-wave superconductivity.

In this new basis, the Bogoliubov quasiparticle operator is defined as [26]:

$$\gamma_{\mathbf{k}}^{(E)\dagger} = u_{\mathbf{k}\uparrow}^{(E)} c_{\mathbf{k}\uparrow}^{\dagger} + u_{\mathbf{k}\downarrow}^{(E)} c_{\mathbf{k}\downarrow}^{\dagger} + v_{\mathbf{k}\uparrow}^{(E)} c_{-\mathbf{k}\uparrow} + v_{\mathbf{k}\downarrow}^{(E)} c_{-\mathbf{k}\downarrow}, \tag{2.44}$$

where the coefficients $u_{\mathbf{k}\uparrow}^{(E)}$, $u_{\mathbf{k}\downarrow}^{(E)}$, $v_{\mathbf{k}\uparrow}^{(E)}$ and $v_{\mathbf{k}\downarrow}^{(E)}$ are the components of the eigenvectors of the Nambu matrix $\underline{h}_{\mathbf{k}}$ and $E$ denotes the energy of the state. Due to the particle-hole symmetry of the BdG Hamiltonian, these

coefficients are related to each other via [26]:

$$
\begin{bmatrix}
u_{\mathbf{k}\uparrow}^{(E)} \\
u_{\mathbf{k}\downarrow}^{(E)} \\
v_{\mathbf{k}\uparrow}^{(E)} \\
v_{\mathbf{k}\downarrow}^{(E)}
\end{bmatrix}
=
\begin{bmatrix}
v_{-\mathbf{k}\uparrow}^{(-E)*} \\
v_{-\mathbf{k}\downarrow}^{(-E)*} \\
u_{-\mathbf{k}\uparrow}^{(-E)*} \\
u_{-\mathbf{k}\downarrow}^{(-E)*}
\end{bmatrix} .
\tag{2.45}
$$

These relationships combined with Eqn. (2.44) lead to the following interesting feature of the Bogoliubov quasiparticles:

$$
\gamma_{\mathbf{k}}^{(E)\dagger} = \gamma_{-\mathbf{k}}^{(-E)}, \qquad \text{if} \quad E = 0, \quad \mathbf{k} = 0.
\tag{2.46}
$$

Therefore, in the special case of a zero energy state at zero momentum[14], the Bogoliubov quasiparticle is its own antiparticle and, since it obeys the Fermi commutation relations, it is a genuine Majorana fermion. This possibility to form Majorana fermions, caused by the doubling of the basis, should not be seen as a new physical feature of the Bogoliubov quasiparticle. It merely reveals a different side of their nature in this more general formalism[15]. Realisation of Majorana fermions in conventional *s*-wave superconductors is still unfeasible since there are no zero energy states in such a system (see also Fig. 2.3), regardless of the formalism used.

## 2.5.2 Majorana fermions at the ends of a ferromagnetic wire

As shown in the previous Section 2.5.1, Bogoliubov particles can form Majorana fermions at zero energy and $\mathbf{k} = 0$. We will now discuss how to introduce such a zero energy state into the band structure of a *s*-wave superconductor. Then, we will move on to explain why a ferromagnetic chain set-up is beneficial to create strongly localised Majorana fermions.

---

[14]To be more precise, any high symmetry point additionally to $\mathbf{k} = 0$ in the band structure at zero energy can fulfil this condition. For example, the point $\mathbf{k} = \pi = -\pi$ in a one dimensional tight binding model.

[15]For a special kind of superconductivity, so called p-wave which couples electrons with parallel spin, it is possible to write down Bogoliubov quasiparticles that fulfil the condition for Majorana fermions (Eqn. (2.46)) and can be described by a two component Nambu basis.

**Spin-orbit coupled *s*-wave superconductor with Zeeman interaction**
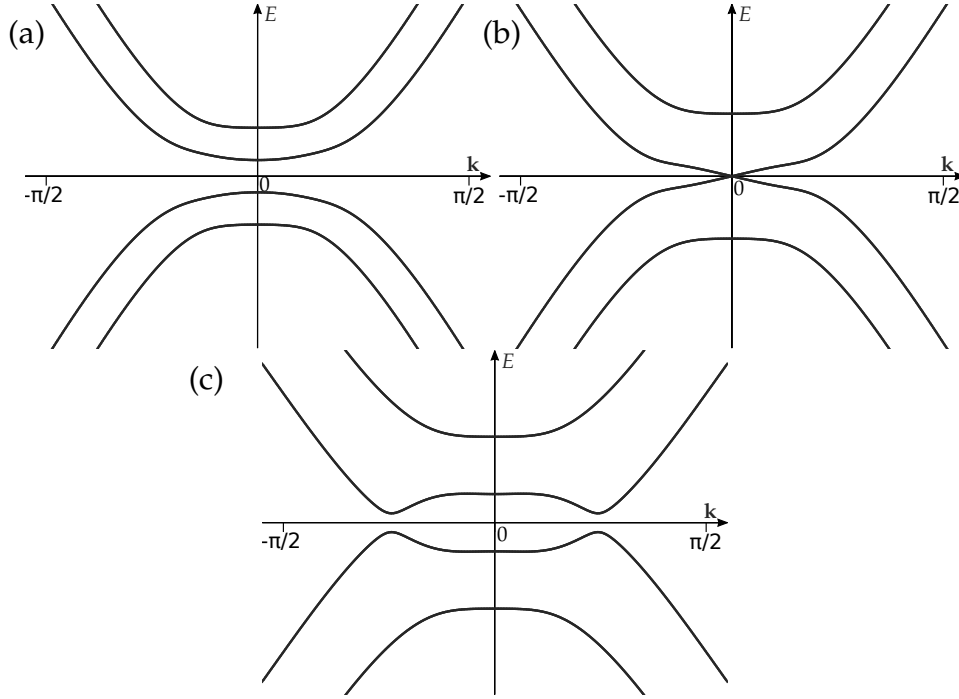


Figure 2.12: Band structures according to Eqn. (2.47) for different values of $V_Z$. (a) $V_Z = 0.15\,t < \Delta$: Topological trivial phase. (b) $V_Z = 0.3\,t = \Delta$: Point of the phase transition, with a Dirac cone at $\mathbf{k} = 0$. (c) $V_Z = 0.6\,t > \Delta$: Topological non-trivial phase. The parameters $\alpha$ and $\mu$ are set to $0.3\,t$ and $-2\,t$, respectively.

In Section 2.4.3, it was shown that a Dirac cone can be introduced into the band structure of an insulator by adding Rashba spin-orbit coupling. In order to achieve the same result in a *s*-wave superconductor, a classical Zeeman interaction has to be added the system. This Zeeman term has the additional advantage of providing the possibility to be able to tune the massgap of the system since it can shift bands with opposite spin in different directions in energy.

To understand the band structure of such a system, we will look at a one-dimensional tight binding model[16]. Within this model, $H_{0\,\mathbf{k}}$ and $\boldsymbol{\Delta}_{\mathbf{k}}$

---

[16]The tight binding model is marginally more complicated than the continuous model

can be written as [25, 80, 81]:

$$H_{0\mathbf{k}} = \epsilon_{\mathbf{k}}\boldsymbol{\sigma}_0 - \mathcal{L}_{\mathbf{k}}\boldsymbol{\sigma}_y - V_Z\boldsymbol{\sigma}_z$$
$$\boldsymbol{\Delta}_{\mathbf{k}} = i\Delta\boldsymbol{\sigma}_y, \tag{2.47}$$

where $\boldsymbol{\sigma}_i$ are denoting the Pauli matrices, $\epsilon_{\mathbf{k}} = -2t\cos(\mathbf{k}) - \mu$ describes kinetic energy of the particles, with $t$ being the hopping strength and $\mu$ the chemical potential. $\mathcal{L}_{\mathbf{k}} = i\alpha\mathbf{k}$ is the Rashba SOC which strength is denoted by $\alpha$ and $V_Z$ is the strength of the Zeeman interaction. The superconducting order parameter $\Delta$ is chosen to be constant for all values of $\mathbf{k}$.

This Hamiltonian has a topological non-trivial phase if $\alpha$ is finite and the other parameters meet the condition [17, 82]:

$$0 < |\Delta| < \sqrt{V_Z^2 - (2t + \mu)^2}. \tag{2.48}$$

Outside this range, the band structure is in a trivial topological phase. For the sake of argument, we will set the chemical potential to $\mu = -2t$ and keep the order parameter constant. In this case, the phase transition appears at $V_Z = |\Delta|$ and by varying the Zeeman strength around this point, the system can be adjusted into and out of the non-trivial phase. In Figure 2.12, an example for the topological trivial and the non-trivial phase are shown, as well as the phase transition at the point $V_Z = |\Delta|$. At the phase transition, a Dirac cone forms at the $\Gamma$ point ($\mathbf{k} = 0$) which fulfils the condition for Majorana fermions (Eqn. (2.46)).

Therefore, by varying the Zeeman interaction $V_Z$, the mass gap of the band structure can be adjusted to be zero, so that the system will host a Dirac cone. A Zeeman interaction can be introduced into the system by applying a magnetic field or by coupling the system to a ferromagnetic material. There is still a caveat; the mass gap does not only depend on the Zeeman term but also on the chemical potential and the hopping amplitude. These parameters can vary in a real system due to impurities, effectively preventing the realisation of a system with constant zero mass gap.

---

shown in Section 2.4.3 but is used here because it is related to the model utilised in our simulations.

### 2.5.3 Zero energy states
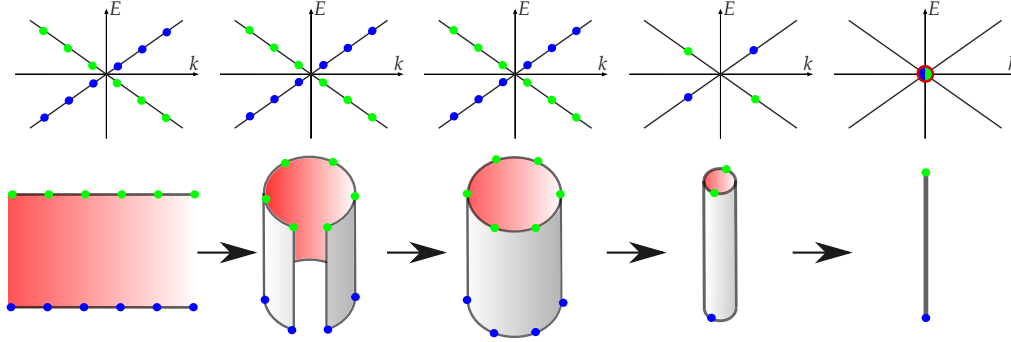


Figure 2.13: From left to right: A finite stripe with a negative mass gap ($M < 0$) embedded in a region with a positive mass gap ($M > 0$). The finite number of states at the boundaries results in a finite number of states on the Dirac cone. By wrapping the stripe to a cylinder and then shrinking it to a line, it leads to a reduction of the edge states of exactly one at each boundary. These two states at the end of the line will lie exactly at the tip of the Dirac cone.

This problem can be circumvented by utilising the bulk-boundary correspondence, as mentioned before in Section 2.4.4. This can be achieved by tuning the mass gap in one part of the system to a negative value by applying a strong enough Zeeman term. The rest of the system is left with a positive mass gap and a Dirac cone will form at the boundary.

The realisation of a finite region leads to another problem in the pursuit of a zero energy state because a finite system will only host a finite number of states that do not necessarily have to lie on the tip of the Dirac cone. In order to understand this more clearly, imagine a finite stripe of a negative mass gap material surrounded by a positive mass gap region (see Fig. 2.13 for a visualisation). The finite number of lattice sites at the boundaries will correspond to a finite number of states on the Dirac cone. For example, if the number of states are even, there will not be a state in the middle of the cone for symmetry reasons. In order to achieve an odd number of states, which would lead to a state at the tip of the cone, one can think of first wrapping the stripe into a cylinder and then shrinking its diameter to zero, i.e. transforming it into a line, leaving only one lattice site at each end. This guarantees that each state at the ends of the line are at exactly zero energy and zero momentum. In terms of our system, Majorana fermions

will appear at the ends of the wire if the line is adjusted into a negative mass gap with the help of a sufficient large Zeeman term. The rest of the system will have a positive mass gap, since it is unaffected by the Zeeman interaction.

This wire set-up has the advantage that the Majorana fermions are highly located at the end of the wire and are, therefore, separated in space which prevents them to annihilate each other given a sufficient wire length.

# 3 Methods

We are examining a two-dimensional $s$-wave superconductor with spin-orbit coupling and a classic Zeeman interaction applied along a line that represents a ferromagnetic wire. The strength of the interaction will be used to adjust the system from a topological trivial into a topological non-trivial phase in the wire region. The focus will lie primarily on analysing the system's local density of the states (LDOS), which is experimentally accessible through scanning tunnelling microscope measurements [28–31]. As discussed in Chapter 2, the Majorana fermions are predicted to occur at the endpoints of the wire if a topological phase is present. In order to detect the Majorana fermions in the LDOS, we will use zero energy states in the LDOS as a smoking gun indicator.

## 3.1 Model Description

### 3.1.1 Hamiltonian

For the simulations, we used a real space Hamiltonian in the Bogoliubov-de Gennes (BdG) formalism [45]. It can be specified in the following form for our particular system [25–27, 59, 80–85]:

$$
\begin{aligned}
H &= H_{kin} + H_{SC} + H_Z + H_{SO} \\
H_{kin} &= -\mu \sum_{\mathbf{i},\sigma} c_{\mathbf{i}\sigma}^{\dagger} c_{\mathbf{i}\sigma} - t \sum_{<\mathbf{i},\mathbf{j}>,\sigma} c_{\mathbf{i}\sigma}^{\dagger} c_{\mathbf{j}\sigma} \\
H_{SC} &= \sum_{\mathbf{i}} \left( \Delta_{\mathbf{i}} c_{\mathbf{i}\uparrow}^{\dagger} c_{\mathbf{i}\downarrow}^{\dagger} + h.c. \right) \\
H_{SO} &= \alpha \sum_{\mathbf{i},\mathbf{b}} \left( e^{i\theta_{\mathbf{b}}} c_{\mathbf{i}+\mathbf{b}\downarrow}^{\dagger} c_{\mathbf{i}\uparrow} + h.c. \right) \\
H_Z &= -\sum_{\mathbf{i},\sigma,\sigma'} V_Z\left(\mathbf{i}\right) \left(\sigma_z\right)_{\sigma\sigma'} c_{\mathbf{i}\sigma}^{\dagger} c_{\mathbf{i}\sigma'}.
\end{aligned}
\tag{3.1}
$$

$c_{\mathbf{i}\sigma}^{\dagger}$ and $c_{\mathbf{i}\sigma}$ are creation and annihilation operators, creating or annihilating particles at the lattice site $i$ with spin orientation $\sigma$. The indexes $<\mathbf{i}, \mathbf{j}>$ are denoting neighbouring sites. The spin index $\sigma$ labels particles with spins up $\uparrow$ or down $\downarrow$ in the $z$-direction, perpendicular to the $x,y$-plane. $\mathbf{b}$ is a vector pointing to a neighbouring site of $\mathbf{i}$ and $\theta_{\mathbf{b}}$ is its polar angle. $\sigma_z$ denotes the third Pauli matrix. All lattice sites $i$ are arranged on a two-dimensional square lattice with periodic boundary conditions.

The kinetic term $H_{kin}$ is governed by the chemical potential $\mu$ and the nearest neighbour hopping amplitude $t$, describing the mobility of the particles. We will set $t = 1$ throughout all the calculations and use it as a natural energy scale, i.e. all energy units will be expressed in terms of $t$. The chemical potential is set to $-4\,t$ for all calculations. $H_{SC}$ describes the superconducting interaction between the electrons with opposite spin and its strength is denoted by the order parameter $\Delta_{\mathbf{i}}$. $\Delta_{\mathbf{i}}$ is allowed to vary spatially within the self-consistent calculations, as described in Section 3.3. For the non-self-consistent calculations, the order parameter is held constant and set to $0.3\,t$ if not stated otherwise. The Rashba-like spin-orbit coupling is determined by $H_{SO}$. Its coupling strength is denoted with $\alpha$ and set to $\alpha = 0.3\,t$.
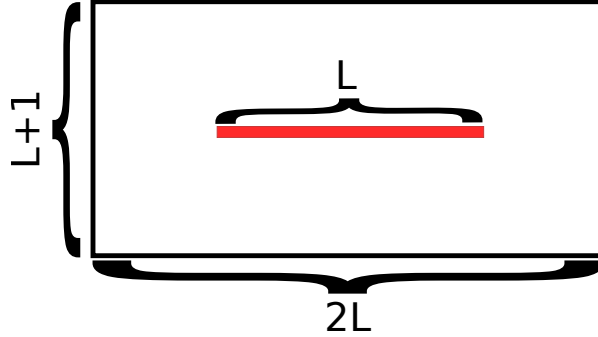


Figure 3.1: Schematic of the two-dimensional system. The Zeeman term $V_Z$ that represents the ferromagnetic wire is applied along the red line in the middle of the system and its length is given by number of lattice sites $L$. The distance from the wire to the boundary is $L/2$.

The ferromagnetic wire that is doped onto the superconductor in experiments is simulated by $H_Z$ as a Zeeman interaction, orientated perpendicular to the plane. The local Zeeman interaction strength $V_Z(\mathbf{i})$ is set to

$V_Z$ along a line in the middle of the system and to zero otherwise. This term is used to adjust the mass gap $M$, so that the wire lattice sites are in a topological non-trivial phase, as discussed in Section 2.5.

The layout of the system is shown in Figure 3.1. For most calculations, the wire length $L$ was chosen to be 30 lattice sites and the distance to the boundary is $L/2$. This measure is necessary to allow the spatially varying order parameter $\Delta_i$ to form a uniform distribution around the edge of the system when doing self-consistent calculations.

We used periodic boundary conditions for all results but checked the results against test cases with non-periodic boundaries.

The calculations are conducted using a real space Nambu spinor basis (analogous to the Nambu basis used in Section 2.5.1):

$$\left( c_{x\uparrow}, c_{x\downarrow}, c_{x\uparrow}^\dagger, c_{x\downarrow}^\dagger \right). \tag{3.2}$$

This basis allows for the treatment of the Hamiltonian (3.1) within a tight binding model since it effectively brings it into a bilinear form. Due to the four component Nambu basis the Hilbert space is $4N$-dimensional, where $N$ is the number of lattice sites ($N = 2L \cdot (L+1)$). To be able to deal with this quadratically growing Hilbert space with respect to the system size, we used the tight binding tool kit (TBTK) which was specially designed to handle such high dimensional problems [37].

The parameters used for the reference calculations are summarised in Table 3.1. The results concerning these parameters will be discussed in Chapter 4.

Table 3.1: Summary of the parameters of the reference system.

| Parameter | Symbol | Value / $t$ |
|---|---|---|
| Chemical potential | $\mu$ | -4 |
| Hopping amplitude | $t$ | 1 |
| Superconducting interaction | $V_{SC}$ | 4.4 |
| Bulk order parameter | $\Delta$ | 0.3 |
| Rashba coupling strength | $\alpha$ | 0.3 |
| Wire length | $L$ | 30 |

We will be focusing mainly on the influence of the Zeeman term strength $V_Z$. We also studied the influence of deviations in the other model parameters but only $\Delta$ and $L$ showed a significant impact on the results and are presented in Sections 4.1.2 and 4.1.3. Changes in $\alpha$ and $\mu$ showed only small contributions to the results and are not shown in this work. The effect of changes in the parameters $\alpha$, $\mu$ and $\Delta$ on the system have also been extensively studied in reference [25].

## 3.2 The tight binding tool kit

The tight binding tool kit (TBTK) [37] is a computational package for solving bilinear Hamiltonians as commonly used in tight binding models. Bilinear Hamiltonians can always be written in the form:

$$H = \sum_{\alpha\beta} a_{\alpha\beta} c_\alpha^\dagger c_\beta, \qquad (3.3)$$

where $\alpha$ and $\beta$ represent arbitrary physical indexes. If all the coefficients $a_{\alpha\beta}$ are known, they can be easily provided to TBTK by using physical indexes. The tool kit takes care of transforming these physical indexes into Hilbert space indexes. The strength of TBTK is that it does this transformation in a very efficient way, sparing the user from doing this explicitly. In the next step one can choose to either use a self written algorithm addressing the physical indexes $\alpha$ and $\beta$ in order to solve the Hamiltonian or simply rely on built-in solvers.

For the implementation of our model Hamiltonian (3.1), we used the following physical indexes: The spatial coordinates $x$ and $y$ for describing the position on the lattice and one index addressing the four components of the Nambu spinor basis, i.e. describing a particle or hole state with either spin index up or down.

We are primarily focusing on the local density of state (LDOS) of the system for various Zeeman term strengths. The LDOS is of particular interest since it can be determined experimentally by scanning tunneling microscope measurements [28–31]. A very effective method to extract the LDOS from a tight binding Hamiltonian is the so called Chebyshev expansion [38, 39] that is discussed in more detail in Section 3.2.1 below.

### 3.2.1 The Chebyshev expansion method

The Chebyshev expansion is a series expressing the single particle Green's functions $G_{\mathbf{ij}}^{\sigma\sigma'}(E)$ of the system [38, 39] and it is related to a Fourier series to some extent. The coefficients of this series can be determined solely by the coefficients $a_{\alpha\beta}$ of the Hamiltonian solely. $G_{\mathbf{ij}}^{\sigma\sigma'}(E)$ is the probability amplitude for a particle to propagate from state $c_{\mathbf{i}}^{\sigma}$ to the state $c_{\mathbf{j}}^{\sigma'}$ at given energy $E$. From these Green's functions, the LDOS can be calculated by [25]:

$$LDOS_{\mathbf{i}}(E) = -\frac{1}{\pi}\sum_{\sigma}\mathrm{Im}\left[G_{\mathbf{ii}}^{\sigma\sigma}(E)\right]. \tag{3.4}$$

The advantage of using the Chebyshev expansion is that its coefficients can be very efficiently calculated with graphical processing units (GPUs), utilising their computational strength of doing matrix multiplications [26]. This allowed us to study systems with wire lengths of up to 40 lattice sites while using the self-consistent method.

The disadvantage of this method is that, due the nature of a series expansion, it has to be truncated and, therefore, it is only an approximation to the exact solution[1]. For our simulations, the Chebyshev expansion was truncated after $10^4$ coefficients and results showed no significant differences when compared to solutions of exact solvers for some test cases.

## 3.3 The self-consistent approach

Superconductors are susceptible to magnetic fields. This means that if a superconductor is exposed to a magnetic field, the order parameter is suppressed and for high enough magnetic fields, the superconductivity of the material will vanish. Superconductivity and magnetic fields can be seen as counterparts, as the former aligns the electron spins antiparallel in order to form Cooper pairs and the latter arranges spins parallel[2].

---

[1]The exact solution, within numerical errors, can be obtained by diagonalising the Hamiltonian. This approach has the downside of being computationally more expensive and, therefore, being unfeasible for bigger system sizes.

[2]Strictly speaking this only true for superconductors with spin-singlet pairing, i.e. antiparallel pairing, as it is the case for conventional s-wave superconductors. On the

Therefore, if the influence of the magnetic field is significantly higher than the superconducting interaction, it is energetically unfavourable for the system to form Cooper pairs and the superconducting characteristics of the material disappear.

The classical Zeeman interaction $H_Z$ simulates such a magnetic field, this means that the superconducting order parameter is expected to be suppressed in its vicinity. To account for this effect, we apply a self-consistent approach to our simulations, as described below.

Starting with an initial guess for the spatial distribution of the order parameter $\Delta_{\mathbf{i}}^{(0)}$, we can extract the pair function $F_{\mathbf{i}} = \frac{1}{N} \langle c_{\mathbf{i}\downarrow} c_{\mathbf{i}\uparrow} \rangle$ from the Hamiltonian using the Chebyshev method[3]. Analogous to the $\mathbf{k}$-space formulation of Eqn. (2.11), $\Delta_{\mathbf{i}}$ can be determined through [26]:

$$\Delta_{\mathbf{i}} = -V_{SC} F_{\mathbf{i}}, \tag{3.5}$$

where $V_{SC}$ is the superconducting interaction strength. It was set to $V_{SC} = 4.4\,t$, resulting in the value for $\Delta$ to be $0.3\,t$ within the unperturbed bulk region (see Tab. 3.1). This new order parameter $\Delta_{\mathbf{i}}^{(1)}$, calculated from $F_{\mathbf{i}}$, is then used as an initial guess for the order parameter distribution of the system. By redoing the whole process of solving the Hamiltonian using $\Delta_{\mathbf{i}}^{(1)}$ a new guess $\Delta_{\mathbf{i}}^{(2)}$ can be obtained. This procedure was repeated until the relative error $\varepsilon^{(n)}$ between two iterations was below a threshold of $10^{-4}$ and the resulting local distribution of $\Delta_{\mathbf{i}}$ was then used for the calculation of the LDOS. The relative error is defined as:

$$\varepsilon^{(n)} = \max_{\mathbf{i}} \left( \left| \frac{\Delta_{\mathbf{i}}^{(n)} - \Delta_{\mathbf{i}}^{(n-1)}}{\Delta_{\mathbf{i}}^{(n)}} \right| \right), \tag{3.6}$$

where $n$ denotes the iteration number.

When doing simulations where only one parameter is changed through a certain range with only small increments, the convergence speed of the self-consistent method can be increased by using the resulting $\Delta_{\mathbf{i}}$ of a previous calculation as the initial guess $\Delta_{\mathbf{i}}^{(0)}$ for the next calculation.

---

other hand, superconductors with spin-triplet pairing are less sensitive to magnetic fields.

[3]TBTK provides an implemented function for this task.

# 4 Results

In this chapter we will set out to discuss three main questions. Firstly, we examine the differences between results with and without using the self-consistent method and review if the additional computational expenses of this method are justified. Secondly, we address the localisation of the Majorana fermion and explain the discrepancy between our findings and previous predictions. Finally, we explore the interaction that causes Majorana fermion states to hybridise at higher Zeeman coupling strengths and describe a mechanism that could lead to communication pathways between the pair of Majorana fermions.

Before we address these questions, we explain the behaviour of the system for increasing Zeeman term strengths and discuss the influence of other important parameters on the result.

## 4.1 System behaviour for different parameter ranges

### 4.1.1 System dependency on the Zeeman coupling strength

In order to show the behaviour of the system for increasing Zeeman term strengths $V_Z$, we plot the local density of states and the local order parameter $\Delta_{\mathbf{i}}$ along an axis cutting through the wire in Figure 4.1 for three different values of $V_Z$ (see also Fig. 3.1 for the system layout).

For values of $V_Z < 1\,t$, the whole system is in a topological trivial phase (Fig. 4.1(a)). Outside the wire region at wire positions $x \ll 15$ and $x \gg 45$, a typical density of states of a $s$-wave superconductor with additional spin orbit coupling and a band gap of $2\,\Delta$ can be seen. The Zeeman term that is applied from $x = 15$ to $x = 45$ suppresses the order parameter slightly
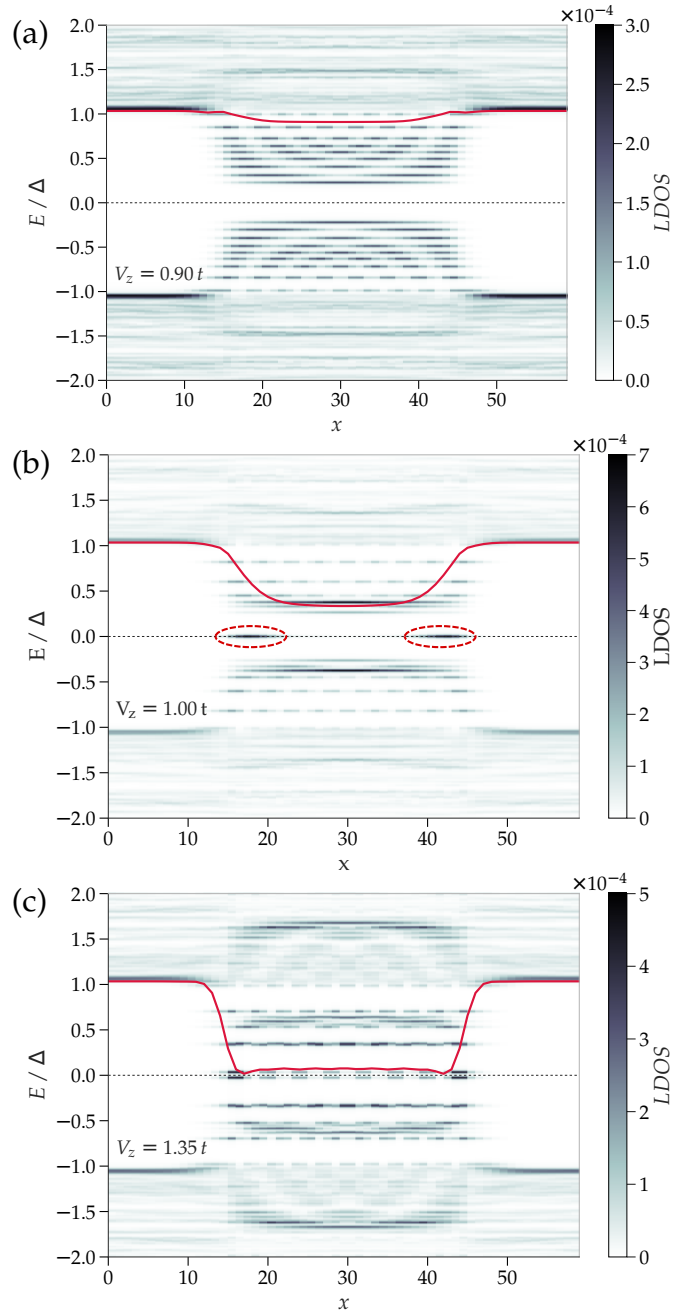
Figure 4.1: Local density of states, their energy and the local order parameter (red line) along an axis cutting along the wire for three different values of $V_Z$. (a) The order parameter is slightly suppressed in the wire region and YSR states can be found in the superconducting gap. (b) LDOS with a topological non-trivial phase along the wire, the Majorana zero energy states are marked by red circles. (c) For relatively high values of $V_Z \geq 1.35\,t$, the order parameter is almost zero at the wire and the Majorana states are hybridising. Note that the mirror symmetry with respect to $E = 0$ is due the nature of the BdG formalism.

in this region, and causes states to move into the band gap[1].

At $V_Z \approx 1\,t$ the system goes through a topological phase transition[2] and the order parameter is significantly suppressed in the wire region. Majorana states occur at both ends of the wire at zero energy and are marked with red circles in Fig. 4.1(b). The system is gapped in energy around these particular states. This is in contrast to an infinite system where a continuous spectrum at the Dirac point would be expected at the topological phase transition. Since our wire length is finite, an energy gap can be observed in our simulations at the phase transition point.

With increasing Zeeman term (Fig. 4.1(c)), the Majorana states start spreading out along the wire and, eventually, due to interactions with other states start hybridising and splitting away from zero energy.

In Figure 4.2 the LDOS at one end of the wire is shown as a function of $V_Z$. Within this representation, the onset of the topological non-trivial phase and the evolution of the Majorana states with increasing Zeeman coupling strengths can be seen more clearly. This graph can be separated in three sections: Into the topological trivial phase $V_Z < 1\,t$ where YSR bands are moving into the band gap, the topological non-trivial phase $1\,t \leq V_Z \leq 1.1\,t$ where Majorana fermions with zero energy exist in the system and the regime $V_Z > 1.1\,t$ where the wire region is still in a topological non-trivial phase, but the Majorana states have finite energy due to interactions with other states. In this region, the Majorana states seem to oscillate with respect to $V_Z$, which is discussed in Sec. 4.4 further on.

The transition to the topological phase takes place at a relatively high Zeeman term strength $V_Z \approx 1\,t$ as compared to an analytically solvable two-dimensional model where $V_Z(\mathbf{i})$ is applied to the whole plane instead of only a line. Within this particular system, the phase transition is predicted to occur at [26, 80] (given that $\mu = -4\,t$):

$$|V_Z| = |\Delta| \tag{4.1}$$

---

[1]Single magnetic impurity sites in conventional superconductors are known to cause localised states within the band gap. This effect is known as Yu-Shiba-Rusinov (YSR) states [59, 86–89]. Our system hosts several of such impurity sites, causing the formation of so called YSR bands in the superconducting gap [25].

[2]The fact that the phase transition occurs at $V_Z \approx 1\,t$ is arbitrary and coincides with the particular choice of parameters.
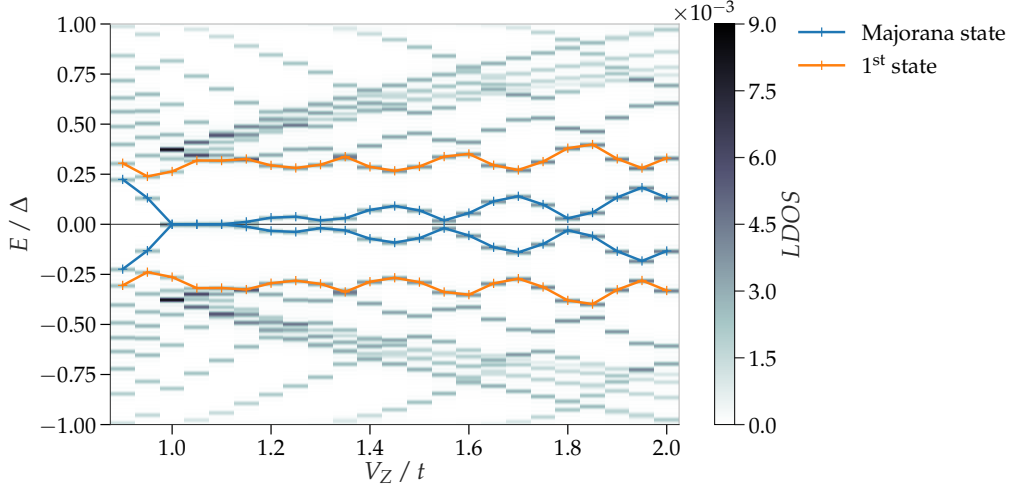
Figure 4.2: Energy and LDOS at the end of the wire for increasing values of $V_Z$. The lines are tracing the energy levels of the Majorana states and the state nearest in energy to them (designated as 1$^{st}$ state).

Therefore, a three times higher Zeeman interaction has to be applied in our simulations compared to this model. That contradiction can be explained by the very high localisation of the Zeeman term to only one lattice site broad line in the simulation. Because of the hopping term, states in the vicinity of the wire that are unaffected by the Zeeman term can leak into the wire region, effectively diluting the influence of the Zeeman interaction. Lattice sites at the ends of the wire are exposed to a higher degree since they have three Zeeman-free-term neighbour sites. Thus, the values of $V_Z$ needed to accomplish a topological phase transition are significantly increased. We discuss this effect again when we are looking at the localisation of the Majorana fermion's wave function in Section 4.3.

## 4.1.2 Wire length

A sufficient length $L$ of the wire is an important factor when it comes to creating Majorana fermions in the system with zero energy. If the wire is too short, the wave functions of the Majorana fermions overlap and, therefore, annihilate each other. This effect can be seen in the LDOS, as Majorana states at finite energies, even though the system is in its
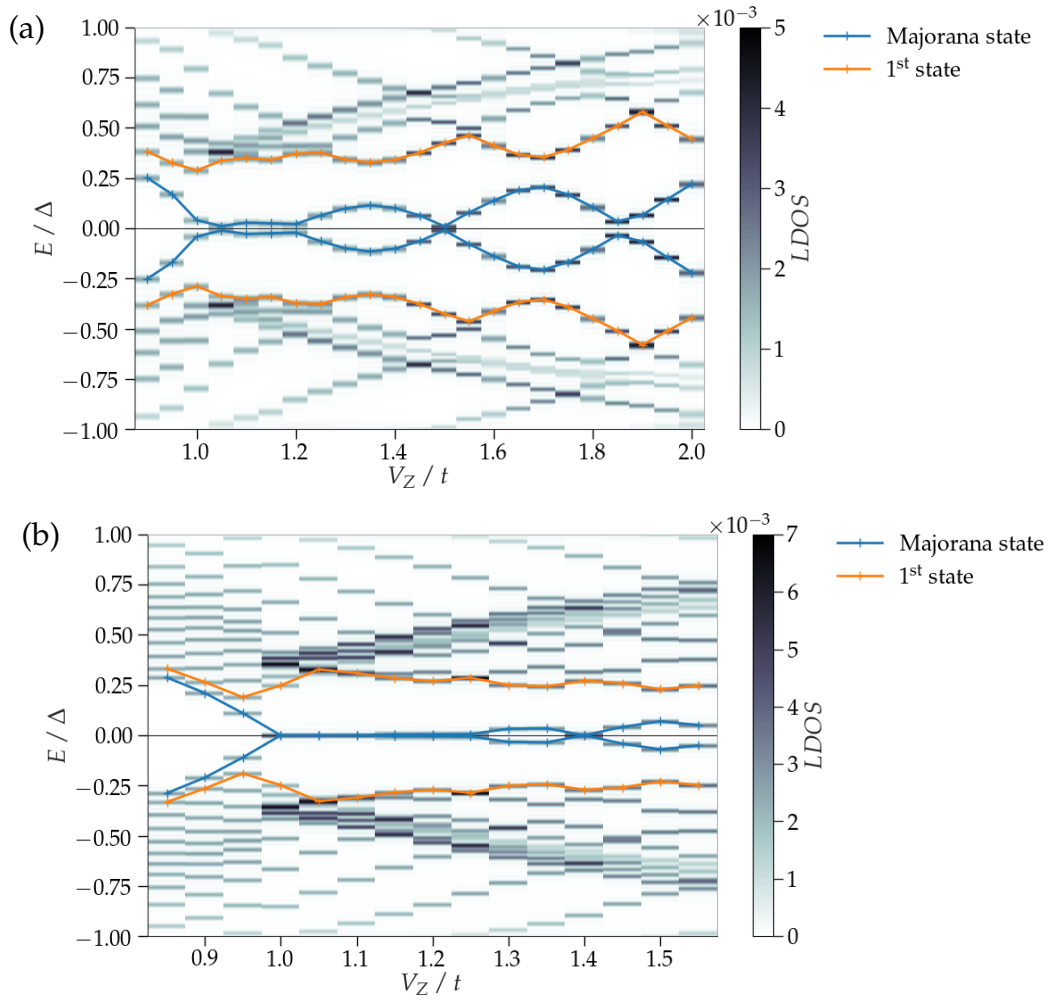
Figure 4.3: Same as Figure 4.2, except for different wire lengths (a) $L = 20$ and (b) $L = 40$.

topological non-trivial phase. Ideally, the wire length should be infinitely long since the wave functions decay exponentially away from the wire ends (cf. Eqn (2.40)). In practice, the overlap of both wave functions is already insignificantly small for relatively short wires. For example, in our simulations, the Majorana fermion states are at approximately zero energy already at wire lengths of approximately $L = 30$.

Figure 4.3(a) shows the evolution of the LDOS for increasing $V_Z$ for a wire length of $L = 20$. This length is found to be too short to support Majorana fermions at zero energy. A longer wire with length $L = 40$ (Fig. 4.3(b)) shows a more stable Majorana fermion as compared to the reference case with a length of $L = 30$.

### 4.1.3 Superconducting interaction strength

Apart from the wire length, a variation of the superconducting interaction $V_{SC}$ shows the highest impact on the simulation results. In order to display its influence on the LDOS, we conducted calculations with an interaction strength of $V_{SC} = 3.2\,t$. This yields a superconducting order parameter in the bulk of $\Delta \approx 0.1\,t$.

A lower order parameter potentially leads to an earlier topological phase transition in terms of Zeeman interaction strength. This can be seen in Figure 4.4[3], where the transition occurs at $V_Z \approx 0.7\,t$. The lower order parameter destabilises the Majorana fermions as it reduces the mass gap (as discussed in Sec. 4.3). This means that their wave function can spread further along the wire and, thus, longer wire lengths are needed to obtain Majorana fermions within the system. For example, a wire of length $L = 30$ embedded in a superconductor with $\Delta = 0.1\,t$ does not support zero energy states (Fig. 4.3(a)), as opposed to a system with $\Delta = 0.3\,t$ (Fig. 4.2). In order to get similar results as in the reference case with $\Delta = 0.3\,t$, a wire of length of $L \approx 40$ or even longer is needed (Fig. 4.3(b)). Since the computational expenses using such a system size would have been too excessive, we decided to use the results for $V_{SC} = 4.4\,t$ and $L = 30$ for the remaining calculations.

---

[3]The lower resolution in the graphs is caused by the fact that the energy is rescaled to $\Delta$. Since $\Delta$ is three times smaller as compared to the other calculations and the effective energy resolution defined by the number of Chebyshev coefficients is the same, the graph appears coarser.
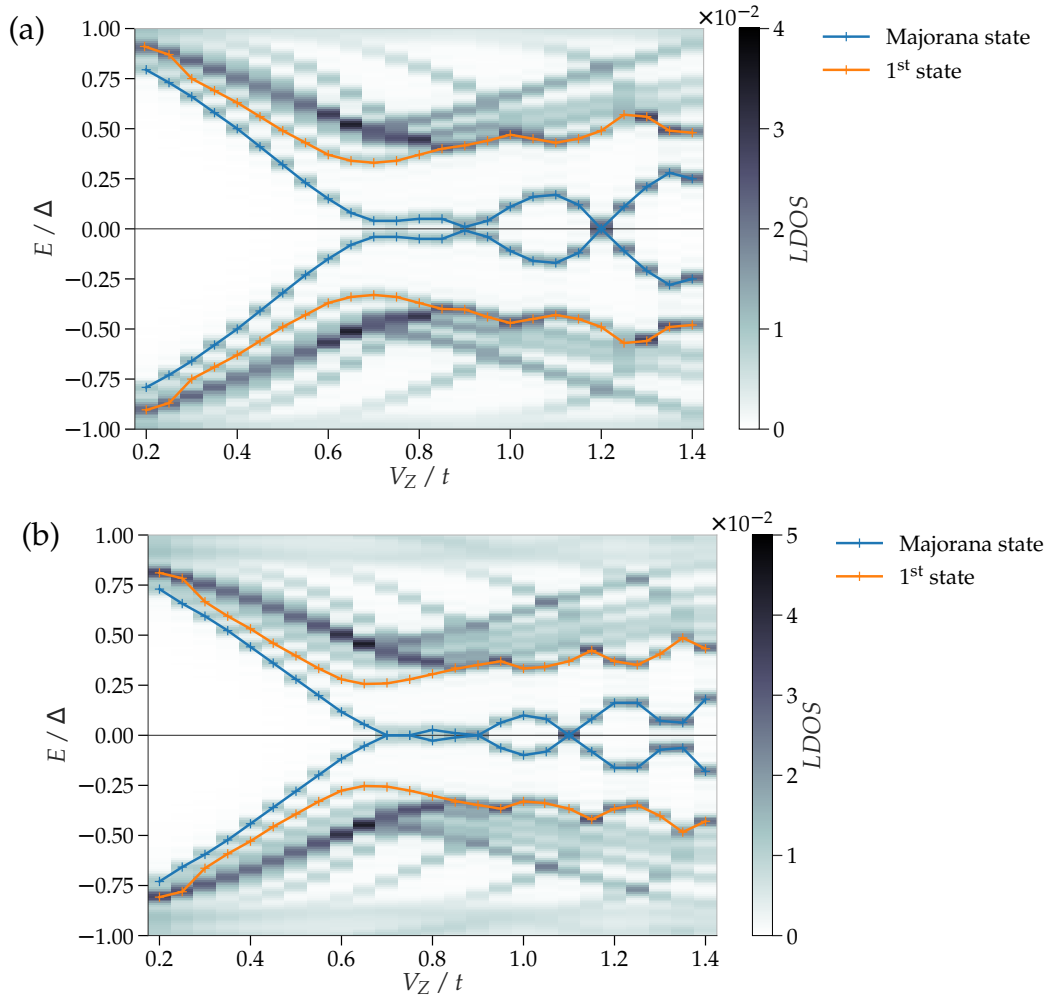
Figure 4.4: Same as Figure 4.2, except for $\Delta = 0.1\,t$ and wire lengths of (a) $L = 30$ and (b) $L = 40$.

## 4.2 Comparison of self-consistent and non-self-consistent results

The self-consistent method is used to capture and simulate the effect of the suppression of the order parameter due to the Zeeman interaction. This is done by iteratively updating the calculation with previous results, as described in 3.3. The number of iterations is typically in the order of 30 to 80. Even though this calculation can be speeded up through various methods, it still comes at a significantly higher computational cost as compared to the non-self-consistent method. This simpler method neglects the local suppression of $\Delta_\mathbf{i}$ and assumes it to be constant throughout the plane. Therefore, it raises the question whether if the additional cost in computational time for the self-consistent method is justified. In this section, we show that this is the case if certain characteristics of the system are of interest. In order to do so, we discuss three major differences found in the results of both methods, namely the robustness of the Majorana fermion with respect to $V_Z$, the mini-gap and the oscillations due to interactions with other states. To compare the results for both methods, we plot the evolutions of the energy of the Majorana states as a function of $V_Z$ in Figure 4.5 (compare to the tracing in Figure 4.2). Additionally, the energy of the sub-gap states closest to the Majorana states are shown as well. We will call these states as first states henceforth.

### 4.2.1 Robustness of the Majorana fermions

We denote the robustness of the Majorana fermions as the range of $V_Z$ over which the Majorana states are at zero energy. The robustness of the Majorana fermion is found to be about four times higher using the non-self-consistent calculations. The zero energy state exists within the range of $V_Z \approx [1.25, 1.7]\, t$, whereas by applying the self-consistent method this range is lowered to $V_Z \approx [1.0, 1.1]\, t$. Another interesting feature is the point where the Majorana fermion is created, which is governed by the topological phase transition, i.e. by the ratio of the effective Zeeman term to the local order parameter on the wire. As one would expect due to the locally suppressed order parameter, the Majorana fermion appears in the self-consistent calculation at a lowered Zeeman term strength $V_Z \approx 1\, t$, as
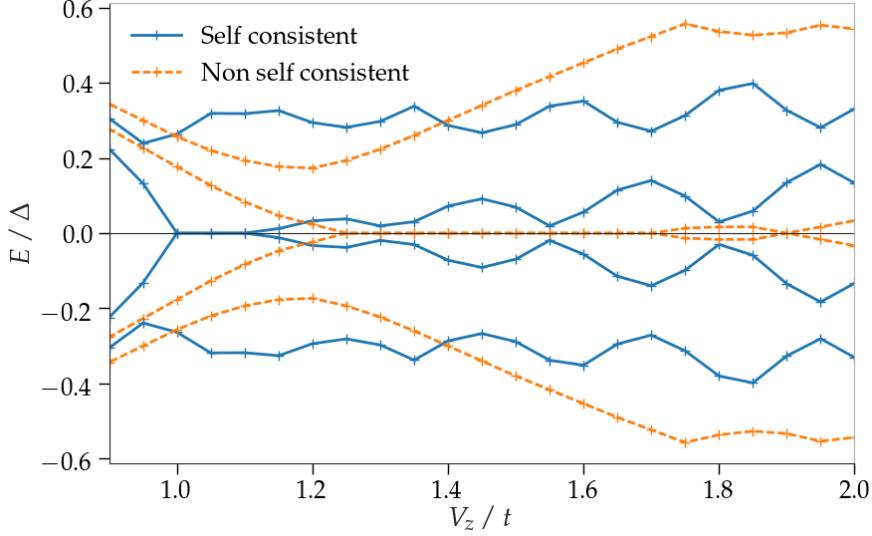
Figure 4.5: Comparison of the energies of the Majorana states (lines closer to zero) and the first closest state to it, for the self-consistent and the non-self-consistent method as a function of $V_Z$. For the non-self-consistent calculation, the superconducting order parameter was held constant at $\Delta = 0.3$, whereas in the self-consistent case the order parameter is 0.3 in the bulk region and was allowed to relax to other values around the wire self-consistently.

compared to the non-self-consistent result of $V_Z \approx 1.25\,t$.

Therefore, the non-self-consistent method suggests a significantly higher robustness for the Majorana fermion than the self-consistent method. This might be a misleading result since the self-consistent calculation is expected to represent more realistic results.

## 4.2.2 Mini-gap

The mini-gap $\Delta E_\gamma$ denotes the energy difference between a Majorana fermion and the first state. This value is of particular interest for quantum computational applications because it is a measure for the stability of information that could be stored in this state. For example, if information would be stored on a Majorana fermion by preparing it in a certain state and if it gets excited to another energy level, this information would be lost. Since real world applications are at finite temperature, this excitation

can always occur within a certain probability due to thermal energy fluctuations. The higher the energy gap, the lower the probability for this process to happen will be. Therefore, a larger mini-gap is more desirable.

We compare the mini-gap for both methods in the range of $V_Z$, where the Majorana fermion is at approximately zero energy. For the self-consistent solution, the mini-gap stays quite constant at energy levels in the range of $\Delta E_\gamma \approx [0.08, 0.1] \, t$, whereas for the non-self-consistent result it increases steadily with $V_Z$ within the value range of $\Delta E_\gamma \approx [0.04, 0.16] \, t$. Therefore, the non-self-consistent results would suggest that the Majorana fermions are thermodynamically more stable for higher values of $V_Z$, which is in contrast to the self-consistent solution, especially in case of longer wires (see Fig. 4.3(b)). The conclusion gained from the former result is particularly misleading in terms of information storage stability because the Majorana fermions might be able to communicate with each other through the first state at larger $V_Z$ values. We explain this effect more comprehensively in Section 4.4.

### 4.2.3 Oscillations of the Majorana state energy

For higher values of $V_Z$, the Majorana zero energy states hybridise and split away from zero energy for both methods. This effect is caused by the interaction of the Majorana states with the first states that are coming close to zero energy as $V_Z$ increases. Due to interactions between those states, however, they are seemingly repelled and move up in energy again. This causes the Majorana states to oscillate with respect to $V_Z$ after a certain threshold (See also Sec. 4.4).

While these oscillations are quite pronounced in the self-consistent solution, they are comparatively weak for the non-self-consistent case. Therefore, the self-consistent method yields clearer results when studying these oscillations in more detail.

## 4.3 Localisation of the Majorana Fermions

The localisation of the Majorana fermion $\xi_M$ was assumed to be in the order of the superconducting coherence length $\xi_{SC}$ [32–34, 52], which is
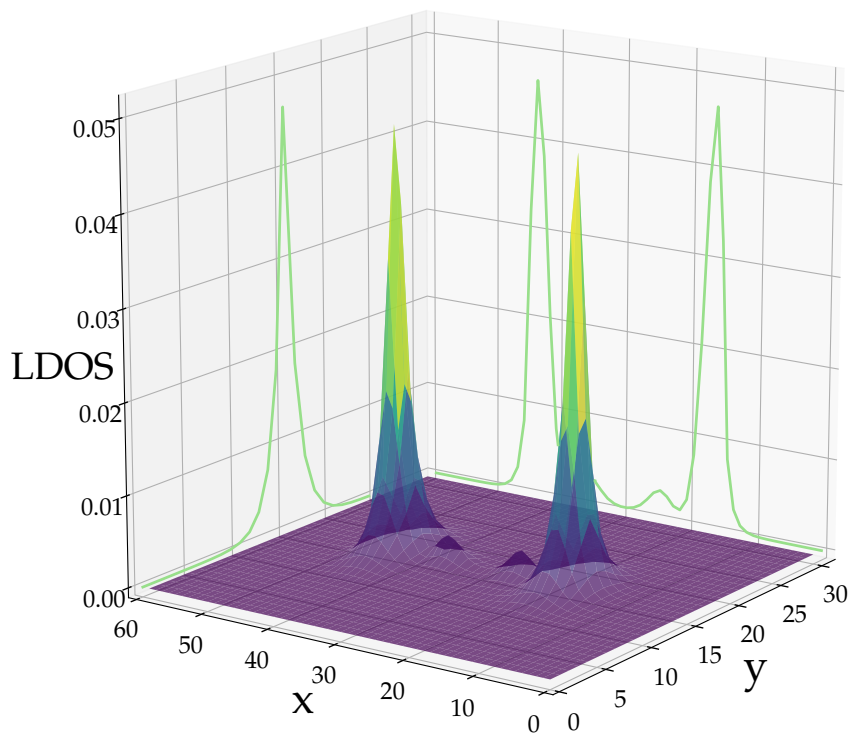
Figure 4.6: The LDOS equal to the probability density $|\psi_M|^2$ of both Majorana fermions plotted for the $(x,y)$-plane.

defined as [60]:

$$\xi_{SC} = \frac{\hbar v_F}{\Delta}, \tag{4.2}$$

where $v_F$ denotes the Fermi velocity of the material. The coherence length is typically in the order of hundreds of lattice sites. For example, for lead it was measured to be 960 Å [90] that accounts for approximately 200 lattice constants [91, 92].

Experiments [28–31], on the other hand, showed that the Majorana fermions at the ends of ferromagnetic wires are localised more strongly than one would suspect from the magnitude of the coherence length. In fact, the Majorana fermions seem to be localised within a few lattice sites. Our calculations are in good agreement with these findings (see Fig. 4.6), indicating that the full width at half maximum (FWHM) of the Majorana probability density along the wire axis is about three lattice constants $a$.

One explanation for this contradiction between theory and experiment was provided by Peng et al. [32] who argued that $\xi_M$ should be scaled down by the coupling strength between the ferromagnetic wire and the superconductor. This approach leaded to similar results for the localisation as measured in experiments. We introduce an alternative approach to explain the nature of the Majorana fermion localisation within this thesis. This explanation is unrelated to the coherence length and instead utilises the mass gap of the band structure to predict the localisation.

Assuming the Majorana fermion wave function can be described analogous to the topological insulator model (see Sec. 2.4.4) as a zero energy edge state, its wave function $\psi_M(x)$ is modelled by [26, 35, 36]:

$$\psi_M(x) \propto e^{\frac{1}{\alpha} \int_0^x M(x')dx'}, \tag{4.3}$$

where $M(x)$ denotes the mass gap of the band structure at position $x$ that is measured along an axis cutting through the wire and is defined to be zero at the point where the mass gap function passes through zero ($M(x = 0) = 0$) at one end of the wire.

In order to be able to estimate $M(x)$, we extracted its value from an analytically solvable problem which is similar to the model Hamiltonian used within this thesis. The difference to this particular model is that the Zeeman term interaction $V_Z(\mathbf{i})$ is held constant throughout the whole system, i.e. the Zeeman interaction is present at every lattice site. The

energy dispersion relationship $E_{\mathbf{k}}$ for this variation of the Hamiltonian is given by [25, 26, 80, 81]:

$$E_{\mathbf{k}} = \pm\sqrt{\epsilon_{\mathbf{k}}^2 + \mathcal{L}_{\mathbf{k}}^2 + V_Z^2 + |\Delta|^2 \pm 2\sqrt{\epsilon_{\mathbf{k}}^2 \mathcal{L}_{\mathbf{k}}^2 + (\epsilon_{\mathbf{k}}^2 + |\Delta|^2)\, V_Z^2}}. \qquad (4.4)$$

The expressions for $\epsilon_{\mathbf{k}}$ and $\mathcal{L}_{\mathbf{k}}$ are the same as in Section 2.5.2. From this expression, the mass gap at $\mathbf{k} = 0$ can be extracted and for our particular choice of parameters, it reads:

$$M = |\Delta| - V_Z. \qquad (4.5)$$

Within this model, the mass gap is constant throughout the system. In order to adapt it to the Hamiltonian used in our simulations, the local values of the order parameter $\Delta_x$ and the Zeeman term $V_Z(x)$ is inserted into Eqn. (4.5), making $M$ dependent of $x$. Another effect that needs to be taken into account is the dilution of the effect of the Zeeman term in the vicinity of the wire (c.f. Sec. 4.1.1). This behaviour is modelled by replacing $V_Z(x)$ with an expression for the effective Zeeman term:

$$V_Z(x) \rightarrow \beta V_Z(x), \qquad (4.6)$$

where $\beta$ is a fit variable that describes the ratio of the applied Zeeman term to the effective Zeeman term. $\beta$ could potentially dependent on $x$ and is expected to be lower around the end of the wire than in the middle. It also varies with other model parameters, foremost $V_Z$. For practical reasons, we approximate $\beta$ to be constant along the wire but still let it be dependent on $V_Z$. These adaptations yield the following expression for $M(x)$:

$$M(x) = |\Delta_x| - \beta V_Z(x). \qquad (4.7)$$

The probability density of an edge state in our particular system is then approximated by:

$$\left|\psi_{M,aprrox}(x)\right|^2 = C \cdot e^{\frac{2}{\alpha} \int_0^x \left(|\Delta_{x'}| - \beta V_Z(x')\right) dx'}, \qquad (4.8)$$

where $C$ denotes another fit parameter that defines the height of the peak value of $\left|\psi_{M,aprrox}(x)\right|^2$.

The probability density of the Majorana state was extracted from the LDOS at its respective energy level, assuming the overlap of the two Majorana wave functions is negligible (Fig. 4.7). In order to show that Eqn. (4.8) can be used to describe the localisation of the Majorana fermion, we fitted Eqn. (4.8) to our simulations. The fit constant $C$ is set equal to the height of the first peak in the probability density of the Majorana states. $\beta$ was by exploiting the fact that the mass gap $M(x)$ is zero at the position of the peak ($x = 0$). This is due to the fact that the peak in the probability density appears exactly at the point where the $M(x)$ changes its sign[4].

$$\beta = \frac{|\Delta_{x=0}|}{V_Z} \tag{4.9}$$

This approximation $\left|\psi_{M,aprrox}(x)\right|^2$ is shown in Figure 4.7 against the LDOS of the Majorana state extracted from the simulations for $V_Z = 1.05\,t$. Both functions show a good agreement for the main peak.

We define the localisation of the Majorana fermion $\xi_M$ as the FWHM of the probability density along the $x$-axis. $\xi_M$ is measured for both the simulations and the approximation and is plotted in Fig. 4.8 (a). The Zeeman term strength range where the Majorana state is at zero energy is shown in green. Both calculations show that the Majorana states become more localised with increasing $V_Z$ and the approximation predicts the overall trend of the simulation up to $V_Z \approx 1.3\,t$. At higher $V_Z$ values, the interactions between the Majorana fermions and other states are more enhanced, rendering the approximation less accurate since it does not take these interactions into account.

The kink in the function of the FWHM of $\left|\psi_{M,aprrox}(x)\right|^2$ at $V_Z \approx 1.35$ is due to a discontinuity in $\Delta_x$ as function of $V_Z$ and is a result of a $\pi$-phase shift in $\Delta_x$ due to interactions [27].

The fact that the Majorana states become more localised with increasing $V_Z$ is in contradiction to the original assumption that the localisation is related to the superconducting coherence length $\xi_{SC}$. To show that this

---

[4]The exponent of Eqn. (4.8) is always negative, except at $x = 0$ where it is zero. Note that $x$ is positive in the direction pointing to the wire, i.e. in the region with negative massgap and, therefore, the sign of the exponent is changed as compared to Section 2.4.4. The point $x = 0$, where the mass gap goes through zero, does not necessarily coincide with the endpoint of the wire due to the Zeeman term dilution effect.
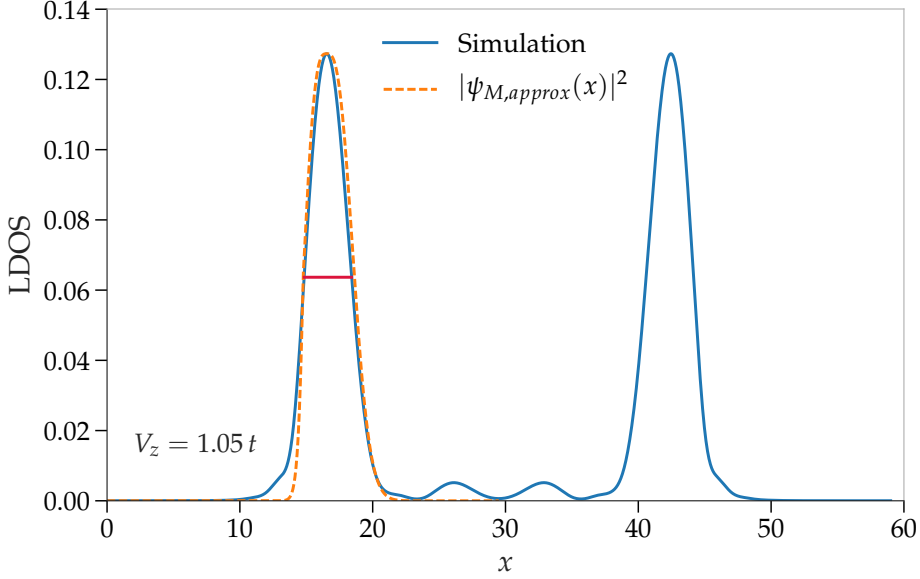
Figure 4.7: LDOS of the Majorana state and the approximation $\left|\psi_{M,aprrox}(x)\right|^2$ for its first probability density peak at $V_Z = 1.05\,t$ as function of the lattice site number along an axis cutting through the wire. The red line marks the FWHM of the probability density. Note that the $x$-axis of the plot does not coincide with the offset of the $x$-coordinate in Eqn. (4.8).

would result in the opposite trend, the following fit function for $\xi_{SC}$ is plotted in Fig. 4.8(b):

$$\xi_{SC} = \frac{C'}{\Delta_x}, \tag{4.10}$$

where $C'$ is fitted to the localisation of the Majorana fermions within the green area.

This prediction is in contrast to our proposed edge state description, as it predicts less localised Majorana states for higher values of $V_Z$. Therefore, we would like to argue that the edge state explanation provides an intuitive explanation for the localisation behaviour of the Majorana state for increasing $V_Z$, accurately predicting a higher localisation for larger Zeeman term strengths.
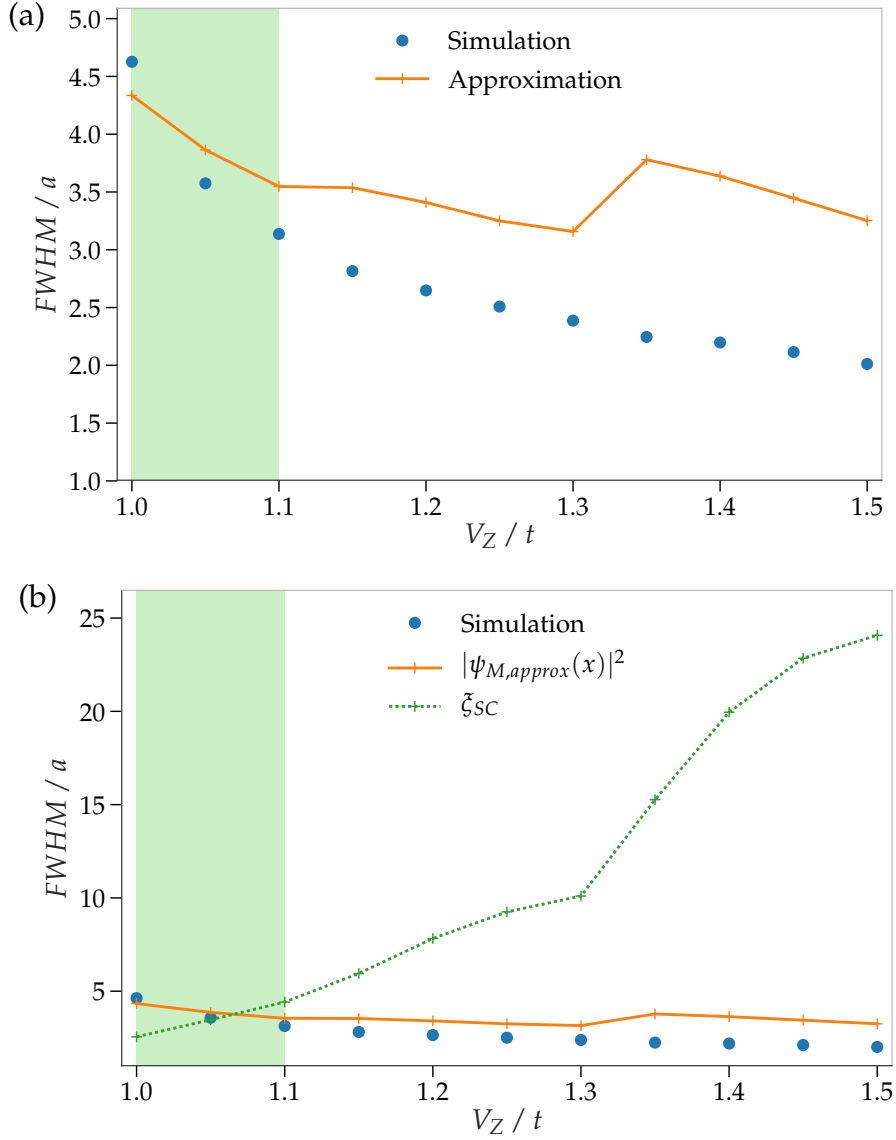
Figure 4.8: FWHM of the Majorana state in units of the lattice constant $a$ for increasing Zeeman term strengths $V_Z$. The green area marks the range of $V_Z$ where the Majorana state is at zero energy. (a) The simulation results are denoted by the dots and the results of the approximation for the probability density by the solid line (Eqn. (4.8)). (b) Additionally to (a), the trend of the coherence length prediction $\tilde{\xi}_{SC}$ is shown (dashed line, Eqn. (4.10)).

## 4.4 Interactions between Majorana fermions and sub-gap states

The assumption that the localisation of the Majorana fermion was related to the coherence length also explained why the Majorana fermions hybridise when the Zeeman term $V_Z$ exceeds a certain level [32–34, 52]. The Zeeman interaction suppresses the superconducting interaction and therefore, increases the coherence length. This means that the Majorana fermions were less localised, causing their wave functions to spread along the wire with increasing $V_Z$. Eventually leading to a significant overlap between the wave functions of the Majorana pair, causing them to annihilate each other.

As we showed in the previous Section 4.3, the opposite is the case. The Majorana fermions become more localised and their wave functions overlap even less at higher values of $V_Z$. This means that a new explanation why the Majorana state shifts away from zero energy is needed. We present a theory that explains the deviation of the states away from zero energy is due to interactions with other states. This is mainly true for the first sub-gap states that come close in space and energy to the Majorana states.

To show that it is possible for these interactions to exist within this system, we start out by explaining what is meant by the first states coming close in space to the Majorana fermions. The principle of locality demands that two states have to be in each other's vicinity to influence each other, i.e. their wave functions have to overlap spatially for the two states to interact. Unfortunately, we are not able to show directly that the wave functions of the Majorana fermions and the first states do overlap. This is caused by restrictions of our simulation method the Chebyshev expansion. It does not allow for calculating the wave function of a state and limits us to observing the LDOS instead. Since the LDOS at the energy of a certain state is equivalent to the absolute value of its wave function, we are able to extract the probability density of a state except for its normalisation. Therefore, we compare the overlap of the probability density instead of the wave functions and assume that these two are similar in value.

In Figure 4.9, the probability density of the Majorana fermion and the first sub-gap state is shown for two values of $V_Z$. For $V_Z = 1.0\,t$, the probability densities of both states have only little spatial overlap (Fig. 4.9

57

(a)), whereas the overlap between both states has significantly increased for $V_Z = 1.25\,t$, (Fig. 4.9 (b)). The spatial overlap between the states allows them to hybridise. This hybridisation can be seen, for example, in Fig. 4.2, where the energies of the Majorana states seem to oscillate as a function of $V_Z$ above a certain threshold. This behaviour is very similar to avoided crossing of states with similar energy and strongly indicates an interaction between the Majorana fermions and other sub-gap states.

The exact origin of these interactions is unknown but their presence in the system can lead to several undesired effects, as presented below. Therefore, exploring their nature could give an insight into how they can be reduced effectively and could present an interesting topic for future research.

An intriguing feature of Majorana fermion states is their resistance to local perturbations. Any change in one Majorana state must also change the second state due to their symmetry. Therefore, any perturbation has to act on both states simultaneously in order to alter them. Since the Majorana fermions are localised at two different locations, namely the end points of the wire, the perturbation must be non-local. If Majorana states couple to a sup-gap state through an interaction, this mechanism can act as a communication pathway between them. A local perturbation can now act on both states at the same time through this communication pathway, effectively lifting the topological protection of the states against local perturbations.

### 4.4.1 Majorana fermions in quantum computing and its problem with interactions

The interactions between sub-gap states and the Majorana fermions can also be problematic when using Majorana fermions in quantum computational applications. For example, one way to use these quasiparticles in quantum computation would be to utilise their non-Abelian behaviour[5]

---

[5]In simple terms, non-Abelian behaviour can occur in a two-dimensional system and it describes particles which obey neither Fermi nor Boson statistics under exchange of particles. For example, when two fermionic or bosonic particles are exchanged, their quantum state acquires a phase factor $e^{i\phi}$, where $\phi = \pi$ for Fermions and $\phi = 0$ for Bosons. For particles with non-Abelian statistics, this phase factor is generally described
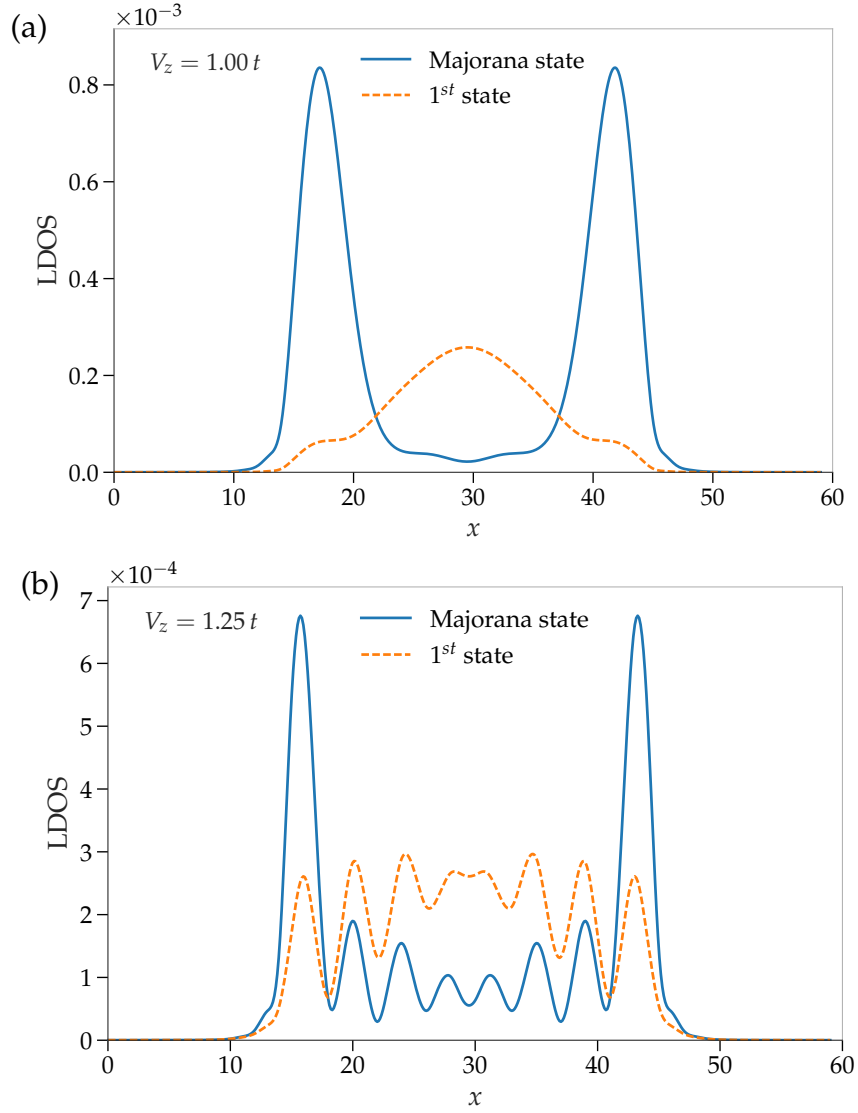
Figure 4.9: LDOS at the energy of the Majorana fermion and of the first state along the wire axis $x$ and two different values of $V_Z$. In this case, the LDOS is equivalent to the probability density of the states. Note that the ringing in subfigure (b) between the Majorana state peaks is caused by hybridisation with other states.

[10, 12, 50, 52, 93] within a method called braiding to form a logical quantum gate [94–98]. In a two-dimensional system, Majorana fermions can pick up a phase factor when they are interchanged. If several of these exchanges are performed with these particles in sequence, the order of these exchanges are important. Different sequences of exchanges lead to different results. A way to imagine this process and the difference between different sequences, is to trace the positions of the particles as a line as they move through time. These lines are usually called world lines within the concept of spacetime. By exchanging the position of these particles, the world lines get twisted against each other and form a kind of weave (hence the name braiding). Depending on the chronological order of the exchanges, this weave will look differently and through changing this order a different outcome can be obtained.

However, if the Majorana fermions interact with other states and gain additional energy, i.e. if they are not at zero energy, they loose their non-Abelian behaviour. Since non-Abelian states are known to be applicable for quantum computational braiding, it is of interest to conserve this characteristic in the Majorana fermions [8]. Furthermore, verifying the non-Abelian behaviour of the Majorana fermions in experiments might be a reliable way to prove if they are present in a system [99–102]. Therefore, it is crucial to keep the interactions minimal and the Majorana fermions at zero energy in experiments. In theory, a simple way to achieve this is to dial the Zeeman interaction $V_Z$ to the topological phase transition value or slightly higher where the mini-gap is the largest and the interactions are negligible. In practice, this might not be feasible since $V_Z$ could depend on the choice of material used for the ferromagnetic wire.

Another potential way to circumvent this hybridisation could be the use of longer ferromagnetic atomic wires. This reduces the overlap between the Majorana states and other sub-gap states since the former are mainly localised at the end of the wires and the latter are more distributed towards the middle section of the wire. The results of Sec. 4.1.2 indicate that this might be the case in our simulations. For example, for $L = 40$ the Majorana fermions are more stable within a larger range of $V_Z$ and the oscillations with respect to $V_Z$ are less pronounced (Fig. 4.3(b)).

---

by a matrix instead. Therefore, exchanges between non-Abelian particles do usually not commute and the sequence of the exchanges is important.

# 5 Conclusion

Majorana fermions are exotic particles that can be created in certain condensed matter systems in the form of quasiparticles. They are of special interest for future quantum computing applications due to their non-Abelian statistics. Systems capable of hosting these special particles usually utilise the bulk-boundary correspondence between two regions of different topology. In this work, we focused on one particular system, i.e. a spin-orbit coupled $s$-wave superconductor interacting with a ferromagnetic adatomic chain. Experiments using this set-up show strong indications for Majorana fermions in scanning tunneling microscope measurements at the end points of the chain.

We simulated this system using a Bogolioubov-de Gennes tight binding model and solved it utilising the tight binding tool kit and the Chebyshev expansion method. We addressed the question if using the self-consistent method is beneficial or whether the non-self-consistent method is able to produce similar results. The former method has the benefit of modelling the local superconducting order parameter more accurately, whereas the latter is computationally less expensive. Our findings showed a significant difference between both methods, especially for certain properties of the system. The mini-gap in energy between the Majorana states and nearest sub-gap state is lower for the self-consistent solution. The parameter range for the coupling strength between the superconducting material and the ferromagnetic chain where the Majorana state is a true zero energy state is considerably reduced. In addition, the oscillations in energy of the Majorana fermions with respect to an increase in this coupling strength are more pronounced when using the self-consistent method. These results underlined the importance of using this computationally more time consuming method if the aforementioned properties are of interest when simulating this kind of system. Furthermore, we showed that the localisation of the Majorana fermion can be modelled by expressing it as an edge state and, therefore, be described by the local mass gap of the band

structure. This contradicts previous phenomenological theories describing the localisation as proportional to the coherence length of the superconductor. Our results also indicate an interaction between the Majarona states and other sub-gap states, causing the former states to hybridise and enabling a communication pathway between them. This has the negative effect of lifting the topological protection against local perturbations of these states. Moreover, interactions can also be problematic for quantum computational applications of Majorana fermions since they can alter their non-Abelian behaviour. In order to understand the exact nature of these interactions and how their influence can be reduced, future research is needed. However, simulations showed that a larger wire length can reduce these interactions and, therefore, stabilise the Majorana fermion states.

# 6 Acknowledgements

# Bibliography

[1] Ettore Majorana. "Teoria simmetrica dell'elettrone e del positrone". In: *Il Nuovo Cimento (1924-1942)* 14.4 (1937), p. 171 (cit. on pp. 1, 14).

[2] Frank Wilczek. "Majorana returns". In: *Nature Physics* 5.9 (2009), pp. 614–618 (cit. on pp. 1, 3, 14).

[3] M Gell-Mann et al. "Supergravity, 1979, 315". In: *North-Holland, Amsterdam, Yanagida T., Sawada O., Sugamoto A., Proceedings of the Workshop on the Unified Theory and the Baryon Number in the Universe*. Vol. 95. 1979, pp. 79–18 (cit. on pp. 1, 14).

[4] T Yanagida. "Proceedings of the Workshop on the Baryon Number of the Universe and Unified Theories, Tsukuba, Japan, 1979". In: (1979) (cit. on pp. 1, 14).

[5] Frank T Avignone III, Steven R Elliott, and Jonathan Engel. "Double beta decay, Majorana neutrinos, and neutrino mass". In: *Reviews of Modern Physics* 80.2 (2008), p. 481 (cit. on p. 1).

[6] S Dimopoulos, S Raby, and Frank Wilczek. "Supersymmetry and the scale of unification". In: *Physical Review D* 24.6 (1981), p. 1681 (cit. on p. 1).

[7] Steven Weinberg. *The quantum theory of fields*. Vol. 3. Cambridge university press, 1999 (cit. on p. 1).

[8] Dmitri A Ivanov. "Non-Abelian statistics of half-quantum vortices in p-wave superconductors". In: *Physical review letters* 86.2 (2001), p. 268 (cit. on pp. 1, 60).

[9] Chetan Nayak et al. "Non-Abelian anyons and topological quantum computation". In: *Reviews of Modern Physics* 80.3 (2008), p. 1083 (cit. on p. 1).

[10]   Jason Alicea. "New directions in the pursuit of Majorana fermions in solid state systems". In: *Reports on Progress in Physics* 75.7 (2012), p. 076501 (cit. on pp. 1, 3, 14, 60).

[11]   A Yu Kitaev. "Fault-tolerant quantum computation by anyons". In: *Annals of Physics* 303.1 (2003), pp. 2–30 (cit. on p. 1).

[12]   CWJ Beenakker. "Search for Majorana fermions in superconductors". In: *Annu. Rev. Condens. Matter Phys.* 4.1 (2013), pp. 113–136 (cit. on pp. 1, 60).

[13]   Grigory E Volovik. *The universe in a helium droplet*. Vol. 117. Oxford University Press on Demand, 2003 (cit. on p. 1).

[14]   Liang Fu and Charles L Kane. "Superconducting proximity effect and Majorana fermions at the surface of a topological insulator". In: *Physical review letters* 100.9 (2008), p. 096407 (cit. on p. 1).

[15]   Liang Fu and Charles L Kane. "Josephson current and noise at a superconductor/quantum-spin-Hall-insulator/superconductor junction". In: *Physical Review B* 79.16 (2009), p. 161408 (cit. on p. 1).

[16]   Roman M Lutchyn, Jay D Sau, and S Das Sarma. "Majorana fermions and a topological phase transition in semiconductor-superconductor heterostructures". In: *Physical review letters* 105.7 (2010), p. 077001 (cit. on p. 1).

[17]   Yuval Oreg, Gil Refael, and Felix von Oppen. "Helical liquids and Majorana bound states in quantum wires". In: *Physical review letters* 105.17 (2010), p. 177002 (cit. on pp. 1, 32).

[18]   Jason Alicea et al. "Non-Abelian statistics and topological quantum information processing in 1D wire networks". In: *Nature Physics* 7.5 (2011), pp. 412–417 (cit. on p. 1).

[19]   S Nadj-Perge et al. "Proposal for realizing Majorana fermions in chains of magnetic atoms on a superconductor". In: *Physical Review B* 88.2 (2013), p. 020407 (cit. on p. 1).

[20]   Falko Pientka, Leonid I Glazman, and Felix von Oppen. "Topological superconducting phase in helical Shiba chains". In: *Physical Review B* 88.15 (2013), p. 155420 (cit. on p. 1).

[21]   Jelena Klinovaja et al. "Topological superconductivity and Majorana fermions in RKKY systems". In: *Physical review letters* 111.18 (2013), p. 186805 (cit. on p. 1).

[22]   Bernd Braunecker and Pascal Simon. "Interplay between classical magnetic moments and superconductivity in quantum one-dimensional conductors: toward a self-sustained topological Majorana phase". In: *Physical review letters* 111.14 (2013), p. 147202 (cit. on p. 1).

[23]   MM Vazifeh and Marcel Franz. "Self-organized topological state with Majorana fermions". In: *Physical review letters* 111.20 (2013), p. 206802 (cit. on p. 1).

[24]   Younghyun Kim et al. "Helical order in one-dimensional magnetic atom chains and possible emergence of Majorana bound states". In: *Physical Review B* 90.6 (2014), p. 060401 (cit. on p. 1).

[25]   Kristofer Björnson and Annica M Black-Schaffer. "Majorana fermions at odd junctions in a wire network of ferromagnetic impurities". In: *Physical Review B* 94.10 (2016), p. 100501 (cit. on pp. 1, 28, 32, 35, 38, 39, 43, 53).

[26]   Kristofer Björnson. "Topological band theory and Majorana fermions". PhD thesis. Uppsala Universitet, 2016 (cit. on pp. 1–3, 11, 14, 25–30, 35, 39, 40, 43, 52, 53).

[27]   Kristofer Björnson, Alexander V Balatsky, and Annica M Black-Schaffer. "Superconducting order parameter $\pi$-phase shift in magnetic impurity wires". In: *Physical Review B* 95.10 (2017), p. 104521 (cit. on pp. 1, 35, 54).

[28]   Stevan Nadj-Perge et al. "Observation of Majorana fermions in ferromagnetic atomic chains on a superconductor". In: *Science* 346.6209 (2014), pp. 602–607 (cit. on pp. 2, 35, 38, 52).

[29]   Rémy Pawlak et al. "Probing atomic structure and Majorana wavefunctions in mono-atomic Fe-chains on superconducting Pb-surface". In: *arXiv preprint arXiv:1505.06078* (2015) (cit. on pp. 2, 35, 38, 52).

[30]   Michael Ruby et al. "End states and subgap structure in proximity-coupled chains of magnetic adatoms". In: *Physical review letters* 115.19 (2015), p. 197204 (cit. on pp. 2, 35, 38, 52).

[31]   Benjamin E Feldman et al. "High-resolution studies of the Majorana atomic chain platform". In: *Nature Physics* (2016) (cit. on pp. 2, 35, 38, 52).

[32]   Yang Peng et al. "Strong localization of Majorana end states in chains of magnetic adatoms". In: *Physical review letters* 114.10 (2015), p. 106801 (cit. on pp. 2, 50, 52, 57).

[33]   Eugene Dumitrescu et al. "Majorana fermions in chiral topological ferromagnetic nanowires". In: *Physical Review B* 91.9 (2015), p. 094505 (cit. on pp. 2, 50, 57).

[34]   Falko Pientka et al. "Topological superconducting phase and Majorana bound states in Shiba chains". In: *Physica Scripta* 2015.T164 (2015), p. 014008 (cit. on pp. 2, 50, 57).

[35]   M Zahid Hasan and Charles L Kane. "Colloquium: topological insulators". In: *Reviews of Modern Physics* 82.4 (2010), p. 3045 (cit. on pp. 2, 3, 14, 21, 25, 27, 52).

[36]   Xiao-Liang Qi and Shou-Cheng Zhang. "Topological insulators and superconductors". In: *Reviews of Modern Physics* 83.4 (2011), p. 1057 (cit. on pp. 2, 3, 14, 27, 52).

[37]   Kristofer Björnson and Andreas Theiler. *dafer45/TBTK: First version with native plotting*. Apr. 2017. DOI: 10.5281/zenodo.556398. URL: https://doi.org/10.5281/zenodo.556398 (cit. on pp. 2, 37, 38).

[38]   Alexander Weiße et al. "The kernel polynomial method". In: *Reviews of modern physics* 78.1 (2006), p. 275 (cit. on pp. 2, 38, 39).

[39]   L Covaci, FM Peeters, and M Berciu. "Efficient numerical approach to inhomogeneous superconductivity: the Chebyshev-Bogoliubov–de Gennes method". In: *Physical review letters* 105.16 (2010), p. 167006 (cit. on pp. 2, 38, 39).

[40]   Henrik Bruus and Karsten Flensberg. *Many-body quantum theory in condensed matter physics: an introduction*. Oxford University Press, 2004 (cit. on pp. 3, 4).

[41]   Alexander Altland and Ben D Simons. *Condensed matter field theory*. Cambridge University Press, 2010 (cit. on p. 3).

[42] Gerald D Mahan. *Many-particle physics*. Springer Science & Business Media, 2013 (cit. on pp. 3, 4).

[43] Piers Coleman. *Introduction to many-body physics*. Cambridge University Press, 2015 (cit. on pp. 3–8, 10–13).

[44] John Robert Schrieffer. *Theory of superconductivity*. Avalon Publishing, 1983 (cit. on p. 3).

[45] Pierre-Gilles De Gennes. *Superconductivity of metals and alloys (advanced book classics)*. Perseus Books Group, 1999 (cit. on pp. 3, 28, 35).

[46] Michael Tinkham. *Introduction to Superconductivity: 2nd Edition*. Dover Books on Physics, 2004 (cit. on pp. 3, 6–8, 28).

[47] Tohru Eguchi, Peter B Gilkey, and Andrew J Hanson. "Gravitation, gauge theories and differential geometry". In: *Physics reports* 66.6 (1980), pp. 213–393 (cit. on pp. 3, 20).

[48] Mark Anthony Armstrong. *Basic topology*. Springer Science & Business Media, 2013 (cit. on p. 3).

[49] A Yu Kitaev. "Unpaired Majorana fermions in quantum wires". In: *Physics-Uspekhi* 44.10S (2001), p. 131 (cit. on p. 3).

[50] Martin Leijnse and Karsten Flensberg. "Introduction to topological superconductivity and Majorana fermions". In: *Semiconductor Science and Technology* 27.12 (2012), p. 124003 (cit. on pp. 3, 14, 60).

[51] B Andrei Bernevig and Taylor L Hughes. *Topological insulators and topological superconductors*. Princeton University Press, 2013 (cit. on pp. 3, 14, 20, 24).

[52] Sankar Das Sarma, Michael Freedman, and Chetan Nayak. "Majorana zero modes and topological quantum computation". In: *arXiv preprint arXiv:1501.02813* (2015) (cit. on pp. 3, 14, 50, 57, 60).

[53] Charles Kittel. *Introduction to solid state*. Vol. 162. John Wiley & Sons, 1966 (cit. on p. 3).

[54] N.W. Ashcroft and N.D. Mermin. *Solid State Physics*. Philadelphia: Saunders College, 1976 (cit. on p. 3).

[55] Rudolf Gross and Achim Marx. *Festkörperphysik*. Walter de Gruyter GmbH & Co KG, 2014 (cit. on p. 3).

[56]     Michael E Peskin and Daniel V Schroeder. "Quantum field theory". In: *The Advanced Book Program, Perseus Books Reading, Massachusetts* (1995) (cit. on p. 4).

[57]     Mark Srednicki. *Quantum field theory*. Cambridge University Press, 2007 (cit. on pp. 4, 25).

[58]     Tom Lancaster and Stephen J Blundell. *Quantum field theory for the gifted amateur*. OUP Oxford, 2014 (cit. on p. 4).

[59]     Sergey S Pershoguba et al. "Currents induced by magnetic impurities in superconductors with spin-orbit coupling". In: *Physical Review Letters* 115.11 (2015), p. 116602 (cit. on pp. 4, 35, 43).

[60]     John Bardeen, Leon N Cooper, and John Robert Schrieffer. "Theory of superconductivity". In: *Physical Review* 108.5 (1957), p. 1175 (cit. on pp. 4, 5, 8, 52).

[61]     Leon N Cooper. "Bound electron pairs in a degenerate Fermi gas". In: *Physical Review* 104.4 (1956), p. 1189 (cit. on pp. 5, 6).

[62]     Emmy Noether. "Invariant variation problems". In: *Transport Theory and Statistical Physics* 1.3 (1971), pp. 186–207 (cit. on p. 10).

[63]     Philip W Anderson. "Random-phase approximation in the theory of superconductivity". In: *Physical Review* 112.6 (1958), p. 1900 (cit. on p. 10).

[64]     Yoichiro Nambu. "Quasi-particles and gauge invariance in the theory of superconductivity". In: *Physical Review* 117.3 (1960), p. 648 (cit. on p. 10).

[65]     NN Bogoliubov, VV Tolmachev, and DV Shirkov. "A new method in the theory of superconductivity". In: *Sov. Phys. JETP* 7 (1958), p. 41 (cit. on pp. 11, 12, 28).

[66]     Paul AM Dirac. "The quantum theory of the electron". In: *Proceedings of the Royal Society of London A: Mathematical, Physical and Engineering Sciences*. Vol. 117. 778. The Royal Society. 1928, pp. 610–624 (cit. on p. 14).

[67]     R Jackiw and P Rossi. "Zero modes of the vortex-fermion system". In: *Nuclear Physics B* 190.4 (1981), pp. 681–691 (cit. on p. 14).

[68] Joel E Moore. "The birth of topological insulators". In: *Nature* 464.7286 (2010), pp. 194–198 (cit. on p. 14).

[69] TO Wehling, Annica M Black-Schaffer, and Alexander V Balatsky. "Dirac materials". In: *Advances in Physics* 63.1 (2014), pp. 1–76 (cit. on pp. 14, 24).

[70] Wikimedia Commons. *Mug and Torus morph.* 2007. URL: https://commons.wikimedia.org/wiki/File:Mug_and_Torus_morph.gif (cit. on p. 15).

[71] Wikimedia Commons. *Connection on sphere.* 2008. URL: https://commons.wikimedia.org/wiki/File:Connection-on-sphere.png (cit. on p. 18).

[72] Andrew N Pressley. *Elementary differential geometry.* Springer Science & Business Media, 2010 (cit. on p. 19).

[73] Michael V Berry. "Quantal phase factors accompanying adiabatic changes". In: *Proceedings of the Royal Society of London A: Mathematical, Physical and Engineering Sciences.* Vol. 392. 1802. The Royal Society. 1984, pp. 45–57 (cit. on p. 20).

[74] DJ Thouless et al. "Quantized Hall conductance in a two-dimensional periodic potential". In: *Physical Review Letters* 49.6 (1982), p. 405 (cit. on p. 20).

[75] Aurelien Manchon et al. "New perspectives for Rashba spin-orbit coupling". In: *Nature materials* 14.9 (2015), pp. 871–882 (cit. on p. 24).

[76] Yu A Bychkov and EI Rashba. "Properties of a 2D electron gas with lifted spectral degeneracy". In: *JETP lett* 39.2 (1984), p. 78 (cit. on p. 24).

[77] James D Bjorken and Sidney David Drell. "Relativistic quantum mechanics". In: (1964) (cit. on p. 25).

[78] Michael E Peskin and Daniel V Schroeder. *An Introduction to Quantum Field Theory (Boulder, CO.* 1995 (cit. on p. 25).

[79] JG Valatin. "Comments on the theory of superconductivity". In: *Il Nuovo Cimento (1955-1965)* 7.6 (1958), pp. 843–857 (cit. on p. 28).

[80]  Masatoshi Sato, Yoshiro Takahashi, and Satoshi Fujimoto. "Non-Abelian topological orders and Majorana fermions in spin-singlet superconductors". In: *Physical Review B* 82.13 (2010), p. 134521 (cit. on pp. 32, 35, 43, 53).

[81]  Kristofer Björnson and Annica M Black-Schaffer. "Probing vortex Majorana fermions and topology in semiconductor/superconductor heterostructures". In: *Physical Review B* 91.21 (2015), p. 214514 (cit. on pp. 32, 35, 53).

[82]  Kristofer Björnson et al. "Spin-polarized edge currents and Majorana fermions in one- and two-dimensional topological superconductors". In: *Phys. Rev. B* 92 (21 Dec. 2015), p. 214501 (cit. on pp. 32, 35).

[83]  Masatoshi Sato, Yoshiro Takahashi, and Satoshi Fujimoto. "Non-Abelian topological order in s-wave superfluids of ultracold fermionic atoms". In: *Physical review letters* 103.2 (2009), p. 020401 (cit. on p. 35).

[84]  Annica M Black-Schaffer and Jacob Linder. "Majorana fermions in spin-orbit-coupled ferromagnetic Josephson junctions". In: *Physical Review B* 84.18 (2011), p. 180509 (cit. on p. 35).

[85]  Kristofer Björnson and Annica M Black-Schaffer. "Vortex states and Majorana fermions in spin-orbit coupled semiconductor-superconductor hybrid structures". In: *Physical Review B* 88.2 (2013), p. 024501 (cit. on p. 35).

[86]  L Yu. "Bound state in superconductors with paramagnetic impurities". In: *Acta Phys. Sin* 21 (1965), pp. 75–91 (cit. on p. 43).

[87]  Hiroyuki Shiba. "Classical spins in superconductors". In: *Progress of theoretical Physics* 40.3 (1968), pp. 435–451 (cit. on p. 43).

[88]  AI Rusinov. "Superconcductivity near a Paramagnetic Impurity". In: *Zh. Eksp. Teor. Fiz. Pisma. Red* 9 (1968), p. 146 (cit. on p. 43).

[89]  AV Balatsky, I Vekhter, and Jian-Xin Zhu. "Impurity-induced states in conventional and unconventional superconductors". In: *Reviews of Modern Physics* 78.2 (2006), p. 373 (cit. on p. 43).

[90]     Richard Francis Gasparovic and WL McLean. "Superconducting penetration depth of lead". In: *Physical Review B* 2.7 (1970), p. 2519 (cit. on p. 52).

[91]     EA Owen and EL Yates. "XLI. Precision measurements of crystal parameters". In: *The London, Edinburgh, and Dublin Philosophical Magazine and Journal of Science* 15.98 (1933), pp. 472–488 (cit. on p. 52).

[92]     Harold P Klug. "A. Redetermination of the Lattice Constant of Lead". In: *Journal of the American Chemical Society* 68.8 (1946), pp. 1493–1494 (cit. on p. 52).

[93]     Tudor D Stanescu and Sumanta Tewari. "Majorana fermions in semiconductor nanowires: fundamentals, modeling, and experiment". In: *Journal of Physics: Condensed Matter* 25.23 (2013), p. 233201 (cit. on p. 60).

[94]     Michael Freedman et al. "Topological quantum computation". In: *Bulletin of the American Mathematical Society* 40.1 (2003), pp. 31–38 (cit. on p. 60).

[95]     Graham P Collins. "Computing with quantum knots". In: *Scientific American* 294.4 (2006), pp. 56–63 (cit. on p. 60).

[96]     Sankar Das Sarma, Michael Freedman, and Chetan Nayak. "Topological quantum computation". In: *Physics Today* 59.7 (2006), pp. 32–38 (cit. on p. 60).

[97]     Don Monroe. "Anyons: The breakthrough quantum computing needs". In: *New Scientist* 1 (2008) (cit. on p. 60).

[98]     Liesbeth Venema. "The dreamweaver's abacus: some experts think that a quantum computation could be plaited like a skein of string. And now they may have found the sorts of string they need, finds Liesbeth Venema". In: *Nature* 452.7189 (2008), pp. 803–806 (cit. on p. 60).

[99]     Sankar Das Sarma, Michael Freedman, and Chetan Nayak. "Topologically protected qubits from a possible non-Abelian fractional quantum Hall state". In: *Physical review letters* 94.16 (2005), p. 166802 (cit. on p. 60).

[100]   Eduardo Fradkin et al. "A Chern-Simons effective field theory for the Pfaffian quantum Hall state". In: *Nuclear Physics B* 516.3 (1998), pp. 704–718 (cit. on p. 60).

[101]   Parsa Bonderson, Alexei Kitaev, and Kirill Shtengel. "Detecting non-Abelian statistics in the $\nu$= 5/2 fractional quantum Hall state". In: *Physical review letters* 96.1 (2006), p. 016803 (cit. on p. 60).

[102]   Ady Stern and Bertrand I. Halperin. "Proposed Experiments to Probe the Non-Abelian $\nu = 5/2$ Quantum Hall State". In: *Phys. Rev. Lett.* 96 (1 Jan. 2006), p. 016802. DOI: `10.1103/PhysRevLett.96.016802`. URL: `https://link.aps.org/doi/10.1103/PhysRevLett.96.016802` (cit. on p. 60).